Anthropogenic perturbations to the atmospheric molybdenum cycle

Wong, Michelle Y.; Rathod, Sagar D.; Marino, Roxanne; Li, Longlei; Howarth, Robert W.; Alastuey, Andres; Alaimo, Maria Grazia; Barraza, Francisco; Carneiro, Manuel Castro; Chellam, Shankararaman; Chen, Yu Cheng; Cohen, David D.; Connelly, David; Dongarra, Gaetano; Gómez, Darió; Hand, Jenny; Harrison, R. M.; Hopke, Philip K.; Hueglin, Christoph; Kuang, Yuan wen

Document Version
Publisher's PDF, also known as Version of record

Link to publication on Research at Birmingham portal

Anthropogenic Perturbations to the Atmospheric Molybdenum Cycle

Michelle Y. Wong[1,2] , Sagar D. Rathod[3] , Roxanne Marino[2] , Longlei Li[4], Robert W. Howarth[2] , Andres Alastuey[5] , Maria Grazia Alaimo[6] , Francisco Barraza[7] , Manuel Castro Carneiro[8] , Shankararaman Chellam[9] , Yu-Cheng Chen[10] , David D. Cohen[11], David Connelly[12], Gaetano Dongarra[6], Darió Gómez[13] , Jenny Hand[14] , R. M. Harrison[15,16] , Philip K. Hopke[17,18] , Christoph Hueglin[19] , Yuan-wen Kuang[20] , Fabrice Lambert[21,22] , James Liang[17], Remi Losno[23] , Willy Maenhaut[24] , Chad Milando[25], Maria Inês Couto Monteiro[8], Yasser Morera-Gómez[26] , Xavier Querol[5] , Sergio Rodríguez[27,28,29] , Patricia Smichowski[13,30] , Daniela Varrica[6] , Yi-hua Xiao[31] , Yangjunjie Xu[23], and Natalie M. Mahowald[4,32]

[1]Cary Institute of Ecosystem Studies, Millbrook, NY, USA, [2]Department of Ecology and Evolutionary Biology, Cornell University, Ithaca, NY, USA, [3]Department of Atmospheric Science, Colorado State University, Fort Collins, CO, USA, [4]Department of Earth and Atmospheric Science, Cornell University, Ithaca, NY, USA, [5]Institute of Environmental Assessment and Water Research (IDEA-CSIC), Barcelona, Spain, [6]Dipartimento Scienze della Terra e del Mare, University of Palermo, Sicily, Italy, [7]School of Geography, University of Otago, Dunedin, New Zealand, [8]Coordenação de Análises Minerais, Centro de Tecnologia Mineral – CETEM, Rio de Janeiro, RJ, Brazil, [9]Department of Civil & Environmental Engineering, Texas A&M University, College Station, TX, USA, [10]National Institute of Environmental Health Sciences, National Health Research Institutes, Miaoli, Taiwan, [11]Australian Nuclear Science and Technology Organisation, Lucas Heights, NSW, Australia, [12]Department of Mathematics, Cornell University, Ithaca, NY, USA, [13]Comisión Nacional de Energía Atómica, Gerencia Química, Buenos Aires, Argentina, [14]Cooperative Institute for Research in the Atmosphere, Colorado State University, Fort Collins, CO, USA, [15]School of Geography, Earth and Environmental Sciences, University of Birmingham, Birmingham, UK, [16]Department of Environmental Sciences/Center of Excellence in Environmental Studies, King Abdulaziz University, Jeddah, Saudi Arabia, [17]Clarkson University, Potsdam, NY, USA, [18]Department of Public Health Sciences, University of Rochester School of Medicine and Dentistry, Rochester, NY, USA, [19]Swiss Federal Laboratories for Materials Science and Technology (EMPA), Dübendorf, Switzerland, [20]Key Laboratory of Vegetation Restoration and Management of Degraded Ecosystems, South China Botanical Garden, Chinese Academy of Sciences, Guangzhou, China, [21]Department of Physical Geography, Pontifical Catholic University of Chile, Santiago, Chile, [22]Center for Climate and Resilience Research, University of Chile, Santiago, Chile, [23]Institut de Physique du Globe de Paris, Université de Paris, Paris, France, [24]Department of Chemistry, Ghent University, Gent, Belgium, [25]School of Public Health, Boston University, Boston, MA, USA, [26]Centro de Estudios Ambientales de Cienfuegos (CEAC), Cienfuegos, Cuba, [27]Izaña Atmospheric Research Centre, AEMET, Santa Cruz de Tenerife, Spain, [28]Estación Experimental de Zonas Áridas, EEZA CSIC, Almería, Spain, [29]Instituto de Productos Naturales y Agrobiología, IPNA CSIC, Tenerife, Spain, [30]Consejo Nacional de Investigaciones Científicas y Técnicas (CONICET), Buenos Aires, Argentina, [31]Research Institute of Tropical Forestry, Chinese Academy of Forestry, Guangzhou, China, [32]Cornell Atkinson Center for Sustainability, Cornell University, Ithaca, NY, USA

Abstract Molybdenum (Mo) is a key cofactor in enzymes used for nitrogen (N) fixation and nitrate reduction, and the low availability of Mo can constrain N inputs, affecting ecosystem productivity. Natural atmospheric Mo aerosolization and deposition from sources such as desert dust, sea-salt spray, and volcanoes can affect ecosystem function across long timescales, but anthropogenic activities such as combustion, motor vehicles, and agricultural dust have accelerated the natural Mo cycle. Here we combined a synthesis of global atmospheric concentration observations and modeling to identify and estimate anthropogenic sources of atmospheric Mo. To project the impact of atmospheric Mo on terrestrial ecosystems, we synthesized soil Mo data and estimated the global distribution of soil Mo using two approaches to calculate turnover times. We estimated global emissions of atmospheric Mo in aerosols (<10 μm in diameter) to be 23 Gg Mo yr^{-1}, with 40%–75% from anthropogenic sources. We approximated that for the top meter of soil, Mo turnover times range between 1,000 and 1,000,000 years. In some industrialized regions, anthropogenic inputs have enhanced Mo deposition 100-fold, lowering the soil Mo turnover time considerably. Our synthesis of global observational data, modeling, and a mass balance

comparison with riverine Mo exports suggest that anthropogenic activity has greatly accelerated the Mo cycle, with potential to influence N-limited ecosystems.

Plain Language Summary Molybdenum (Mo) is an essential trace element that is, important for terrestrial and aquatic ecosystems, as it is required for biological nitrogen fixation and uptake. Mo is carried in particles to the atmosphere from sources such as desert dust, sea spray, and volcanoes resulting in losses and sources to different ecosystems. Atmospheric Mo deposition is essential on long time scales for soils which have lost Mo due to soil weathering, with consequences for nitrogen cycling. Anthropogenic changes to the Mo cycle from combustion, motor vehicles, and agricultural dust, are likely to be large, and have more than doubled sources of Mo to the atmosphere. Locally, anthropogenic changes to Mo in industrialized regions can represent a 100-fold increase in deposition, and may affect nitrogen cycling in nitrogen-limited ecosystems.

1. Introduction

Low bioavailability of molybdenum (Mo), an essential trace nutrient utilized as a cofactor in the nitrogenase enzyme that catalyzes biological nitrogen (N) fixation, can constrain N fixation in terrestrial (Dynarski & Houlton, 2018) and freshwater ecosystems (Glass et al., 2012). N is a limiting nutrient across many ecosystems (e.g., LeBauer & Treseder, 2008; Vitousek & Howarth, 1991; Wang & Houlton, 2009), and in these ecosystems N fixation can enable higher productivity and carbon (C) uptake (Houlton et al., 2008; Thornton et al., 2009). Mo limitation of N fixation has been found in some boreal, temperate, and tropical ecosystems (Perakis et al., 2017; Rousk et al., 2016; Silvester, 1989; Wurzburger et al., 2012), while not in other tropical ecosystems (Wong et al., 2020a). In freshwater systems, Mo availability can also constrain N fixation, nitrate uptake, and thus C assimilation in some lakes (Glass et al., 2012; Romero et al., 2013). Atmospheric deposition is a more important source of Mo than local bedrock weathering in some freshwater systems (Carling et al., 2017). In the absence of Mo, many N-fixing bacteria can synthesize "alternative" vanadium (V) and iron (Fe)-only nitrogenase isoforms (Darnajoux et al., 2019; McRose et al., 2017; Zhang et al., 2016). However, alternative nitrogenases show lower specific activity in laboratory experiments (Eady, 1996) and may be less efficient for N fixation, and it is unknown how widespread their activity is in the environment. Natural atmospheric deposition of Mo may be an essential source of Mo for ecosystems on long (>10,000 year) time scales (Wong et al., 2020b), similar to long-range atmospheric inputs of phosphorus (P) to the Amazon (Yu et al., 2015), but anthropogenic activity may be affecting the magnitude and distribution of Mo to the atmosphere.

Both global emission estimates and local observations suggest large anthropogenic sources of atmospheric Mo (Bozlaker et al., 2013; Hueglin et al., 2005; Nriagu & Pacyna, 1988), with previous syntheses estimating roughly equal contributions from anthropogenic and natural sources (Nriagu, 1989; Nriagu & Pacyna, 1988). Mo is used in alloys, lubricants, and catalysts, and can be a by-product of tungsten and copper mining (NPCS, 2009). Other anthropogenic sources of Mo include petrochemical plants and fossil fuel combustion (Boonpeng et al., 2017; Danadurai et al., 2011), mining facilities (Hernández-Pellón & Fernández-Olmo, 2019), and vehicles which release Mo through engine wear (Gonet & Maher, 2019), lubricating oils (Alves et al., 2015), catalytic converters (da Silva et al., 2008; Dillner et al., 2005), and braking on roads (Fujiwara et al., 2011; Hueglin et al., 2005).

Natural sources of atmospheric Mo such as desert dust, sea-spray aerosols, volcanoes, primary biogenic particles, and wildfires (Nriagu, 1989; Wong et al., 2020b), may have different spatial distributions than anthropogenic sources, such as combustion, vehicle-related emissions, and agricultural dust. In addition, the higher solubility of many elements from anthropogenic aerosols due to their chemical and surface associations, reactions during the combustion processes, higher carbon content, and smaller particle sizes (Desboeufs et al., 2005; Jang et al., 2007; Sedwick et al., 2007; Voutsa & Samara, 2002) suggest that anthropogenic aerosols could impact ecosystems more rapidly than natural aerosols such as desert dust. For example, 15%–50% of the total Mo in coal fly is water-soluble (Izquierdo & Querol, 2012; Moreno et al., 2005). Furthermore, atmospheric processing, such as interaction with sulphate plumes, can increase the solubility of Mo, and may be associated geographically more with anthropogenic sources compared to natural sources (Hsu et al., 2010; Meskhidze et al., 2005).

While the spatial distribution of natural atmospheric Mo deposition and its impact on long-term ecosystem function has been examined (Wong et al., 2020b), no previous studies have modeled anthropogenic Mo sources or compared current deposition estimates with observational data. Natural atmospheric Mo deposition has likely shaped ecosystem function across long timescales, but anthropogenic Mo may have begun to accelerate Mo cycling in the past few decades. We present for the first time a synthesis of the observational and modeling evidence for the anthropogenic perturbation in atmospheric Mo for $PM_{2.5}$ and PM_{10} (atmospheric particulate matter, PM, <2.5 and 10 μm in aerodynamic diameter, respectively), as well as their spatial distribution, and discuss the potential impact of anthropogenic Mo on terrestrial ecosystems. We focus on $PM_{2.5}$ and PM_{10} because they are commonly measured in the atmosphere as well as included in the model used here (Mahowald et al., 2014; Ryder et al., 2019).

2. Materials and Methods

2.1. Atmospheric Observations

2.1.1. Description of Atmospheric Observations

To synthesize observational atmospheric Mo data, we collected data from multiple observational networks and sites that record particulate matter (PM) atmospheric concentrations, some of which include elemental and/or chemical speciation. Observations were taken using several different methods and span many years as described in each paper for each set of observations (Figure 1; Data Set S1). From a compilation of these observations (Supporting Information Supplementary Methods), we can both infer the sources from a compositional analysis and by comparing observations against model predictions (Figure 1; Data Set S1). We compiled observations of aerosols in both the $PM_{2.5}$ and PM_{10} size categories (PM < 2.5 and 10 μm in aerodynamic diameter, respectively) (Mahowald et al., 2011) when available. The most common method for sample collection was by filter sampling, separating aerosols into $PM_{2.5}$ and PM_{10}. For Mo quantification, X-ray fluorescence was most commonly used. Further methods and descriptions for each site, along with other elemental data, total particulate matter, and chemical composition are discussed within the respective studies (Figure 1; Data Set S1).

We focus on $PM_{2.5}$ and PM_{10} because they are commonly measured in the atmosphere as well as included in models because of the longer residence time of aerosols <10 μm, although there is evidence that the larger particles can travel long distances as well (Mahowald et al., 2014; Ryder et al., 2019). Instead of measuring PM_{10} and $PM_{2.5}$, some stations measured coarse PM ($PM_{10-2.5}$, mass of particles with aerodynamic diameters between 2.5 and 10 μm) along with fine ($PM_{2.5}$). If both fine and coarse modes were measured at a site, they are summed and compared as if they were PM_{10} observations (Figure 1). Some observational networks or sites were unable to quantify Mo if concentrations were lower than their detection limits. We note that there are many sites, such as from the Interagency Monitoring of Protected Visual Environments (IMPROVE) remote/rural network in the US, which focus only on $PM_{2.5}$ (Hand et al., 2017, 2019), with less than 50% of the Mo values above the detection limit (Figure 1).

For PM_{10} and $PM_{2.5}$, samplers can differ in the sharpness of their size cutoff (Hand et al., 2019). For example, comparisons between collocated sites from the US EPA and IMPROVE suggested that the coarse aerosol mass ($PM_{10-2.5}$) from the EPA sites were 10% higher than at IMPROVE sites, with a 28% difference between these estimates (Hand et al., 2019). The correlation coefficient was 0.9 with a slope of 0.9, suggesting overall a good agreement, although the different biases between samplers should be kept in mind while evaluating Mo atmospheric concentrations both in the PM_{10} and $PM_{2.5}$ size fractions (Hand et al., 2019).

While we focused on observational data for PM_{10} and smaller particles based on the size modes that our model simulates, we also collected bulk/total atmospheric (dry and wet) deposition data (all particle sizes) in the supporting information (Figure S5) to compare to our model simulations. Bulk/total atmospheric deposition also has an ecological impact as it includes all particles that can be distributed to the atmosphere. However, we note that these data are not directly analogous to the model, and that absolute dry and wet deposition rates are often difficult to measure robustly (Heimburger et al., 2012; Prospero et al., 1996).
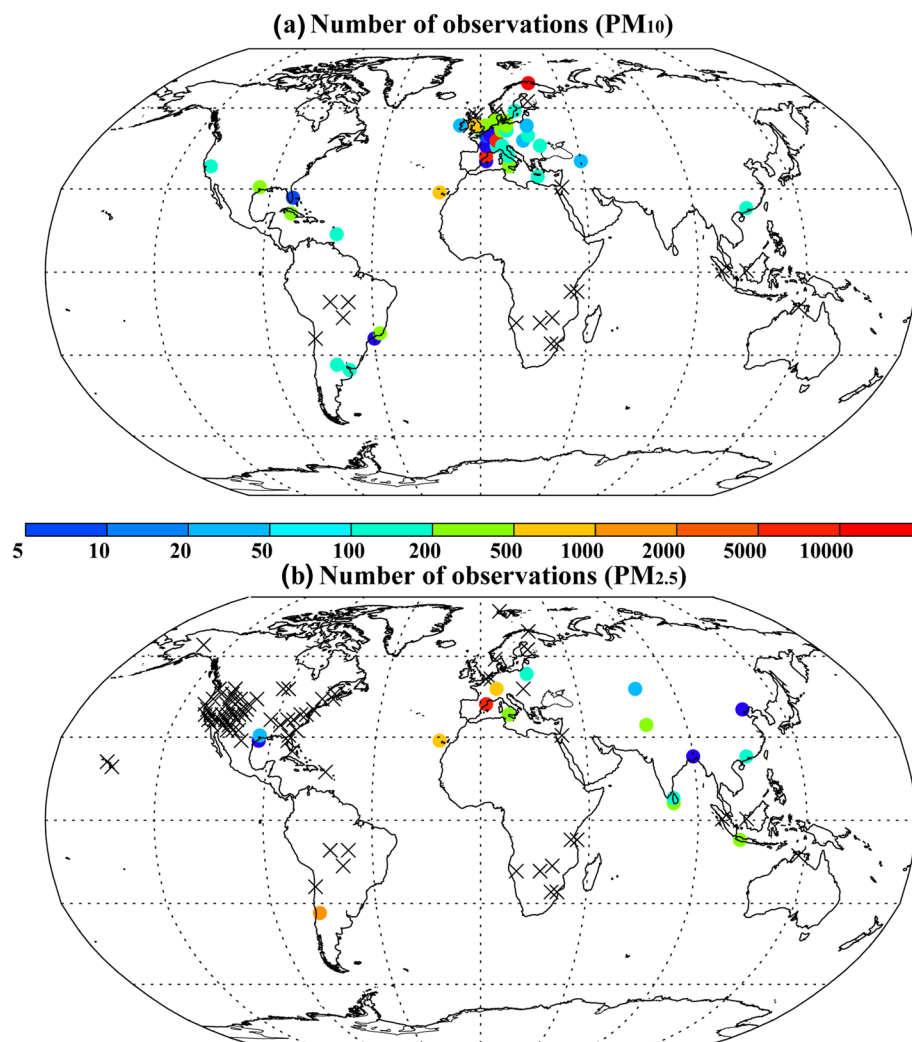
Figure 1. (a) The number of molybdenum (Mo) concentration observations (PM$_{10}$) and (b) the number of number of Mo concentration observations (PM$_{2.5}$) above the detection limit at each site. Observations collected at sites within a 2° × 2° grid box are compiled. Sites with no values above detection levels are represented by an "×." For the sites that measured coarse (PM$_{10\text{-}2.5}$) and fine (PM$_{2.5}$) observations instead of PM$_{2.5}$ and PM$_{10}$, we summed those observations and categorized those sites as PM$_{10}$. Details on the studies and methods are included in the supporting information (Data Set S1) as well as the respective studies (Alastuey et al., 2016; Andreae et al., 2002; Atanacio & Cohen, 2020; Barraza et al., 2017; Bozlaker et al., 2019, 2013; da Silva et al., 2008; DEFRA, 2020; Derimian et al., 2006; DFM and WSP, 2020; Dongarrà et al., 2010, 2007; European Monitoring and Evaluation Programme, 2020; Fuzzi et al., 2007; Gianini et al., 2012a, 2012b; Hand et al., 2017; C. Y. Hsu et al., 2016; Hueglin et al., 2005; Laing et al., 2014b, 2014a; W. Maenhaut & Cafmeyer, 1998; W. Maenhaut et al., 1996a, 1996b, 1996c, 1997a, 1997b, 1999, 2000a, 2000b, 2002a, 2002b, 2005, 2008, 2011; Mkoma et al., 2009a, 2009b, 2009c; Morera-Gómez et al., 2018; Nyanganyura et al., 2007; Pérez et al., 2008; J. P. Putaud et al., 2010, 2004; Rodríguez et al., 2015, 2011; Salma et al., 1997; Smichowski et al., 2004; Swap et al., 2002; Vanderzalm et al., 2003; Van Dingenen et al., 2004; Virkkula et al., 1999; Xiao et al., 2014).

2.1.2. Analysis of Atmospheric Observations

Annual means of atmospheric observations at each site were calculated for all values above the detection limit at each station and reported here. Because Mo concentrations are usually low in atmospheric aerosols (<1 ng m^{-3}), we considered whether we were biasing our results toward higher values because in some cases, a large proportion of the data were below the detection limit. If more than 50% of values at a site were reported as above the detection limit, we used one-third of the minimum detection limit for any samples below the detection limit. However, if less than 50% of the data at a site were above the detection limit, we excluded the data in our annual values. Instead, we included the data to calculate an upper bound using

their respective detection limits. Here, we present both the average values (that include more than 50% of the values above the detection limit), as well as bounded values that include the upper bound of studies with more than 50% of samples under the detection limit (Data Set S1).

In order to compare the model to observational data, records from the observations from different sites were combined into a mean within a grid cell that was two times the model resolution, or 2° × 2°. This process averages the observations over a spatial scale appropriate for comparison with the model (Schutgens et al., 2016). We used the same procedure to count the number of observations in each grid cell (Figure 1).

We conducted an additional analysis at stations from a network in Switzerland (Hueglin et al., 2005) using compositional analysis (Qu et al., 2020). These sites were chosen because of the high spatial and temporal resolution and clear detection limits. We processed the atmospheric concentrations of different elements with the "compositions" package (R Core Team, 2018; van den Boogaart et al., 2014) which provides the "acomp" function, transforming concentrations prior to a principal component analysis to create a biplot (Figure S2). The outcome of this approach is a simple visual analysis of the similarities and differences between the elemental content in PM over time or space, displaying the relative variation more readily and allowing us to assess potential sources of Mo which may vary over space and time.

2.2. Atmospheric Modeling

We simulated atmospheric Mo emission, transport, and deposition in a new Mo module developed based on the aerosol parameterizations within the Community Atmosphere Model, version 6 (CAM6), the atmospheric component of the Community Earth System Model (CESM) developed at the National Center for Atmospheric Research (NCAR) (Hurrell et al., 2013; Liu et al., 2011; Scanza et al., 2015). Simulations were conducted for 6 years, with the last 5 years (2007–2011) used for the analysis (Computational and Information Systems Laboratory, 2019). The model simulates three-dimensional transport and wet and dry deposition for gases and aerosols based on MERRA2 winds (Gelaro et al., 2017). The model included prognostic dust, sea salts, black carbon, organic carbon, and sulphate aerosols in the default version using a modal scheme (Liu et al., 2011). For this study, we added the ability to carry Mo. Between CAM5 and CAM6, the size bounds of the coarse mode were reduced in the default version to better simulate stratospheric aerosols from volcanic eruptions. For this study, the coarse mode size was returned to the CAM5 size to better simulate coarse mode aerosols. Note that we used a different model version (CAM6) than used in Wong et al. (2020b) (CAM4), and thus the magnitude of natural sources changed compared to that study.

Uncertainties in source strengths were large for both the natural sources (desert dust, sea-salt aerosols, volcanoes, primary biogenic particles, and wildfires) and the anthropogenic sources (combustion, braking, and agricultural dust). Therefore, we included a range of values (typically a factor of 10) for the global total based on the range in source Mo concentrations (Table 1). In some simulations, we also included a "high" anthropogenic scenario to test if the model better explained the observational data (Table 1).

2.2.1. Desert Dust

For Mo in desert dust, we assumed a constant fraction of Mo (1.1 mg Mo kg^{-1}) in dust reported by Wong et al. (2020b), well within the range of the crustal abundance of Mo at 1–2 mg Mo kg^{-1} (Rudnick & Gao, 2003; Taylor & McLennan, 1995) which is slightly lower than the 2–5 mg Mo kg^{-1} used in the review of Nriagu (1989) (Table 1). In the CAM model, mineral dust is entrained into the atmosphere in unvegetated dry, arid regions with easily erodible soils during strong near-surface wind events (Zender et al., 2003). The Modal Aerosol Model (Liu et al., 2011) includes three size modes corresponding to the Aitken, accumulation, and coarse modes. We used the CAM5 mass median diameter and sigma as well as the edges of the coarse mode instead of the CAM6 to better simulate the coarse mode and accumulation mode separately, following Li et al. (2020). In each aerosol size mode, Mo was transported and deposited separately using the size fractionation proposed by Albani et al. (2014). The default CAM6 model was modified to use the Kok dust emission scheme (Kok et al., 2014a, 2014b) and tuned to a global mean global aerosol optical depth (AOD) of 0.030 (Li et al., 2020) as suggested to better match observations (Ridley et al., 2016). The dust

Table 1
Concentrations of Mo in Sources and Atmospheric Mo Budgets Based on Simulations From the Community Atmosphere Model (CAM) (v6)

Source	Mo composition (mg kg^{-1})	Composition citation	Global source Mo (Gg yr^{-1}) [ranges] (% fine)	Global source Mo (Gg yr^{-1}) (Nraigu, 1989; Nriagu & Pacyna, 1988)
Natural sources: dust	1.1 Mo/dust	Wong et al. (2020b)	6.8 [3.3–33] (1)	0.12–2.5
Sea-salt aerosols	0.29 Mo/sea-salt aerosol	Wong et al. (2020b)	0.75 [0.38–3.8] (3)	0.01–0.43
Volcanoes	400 Mo/S	Nriagu (1989) and Wong et al. (2020b)	0.71 [0.35–3.5] (100)	0.04–0.75
Primary biogenic particles	1.0 Mo/PBP	Nriagu (1989)	0.49 [0.25–2.5] (10)	0.04–0.75
Wildfires	1,000 Mo/BC	Nriagu (1989)	0.02 [0.01–0.1] (81)	0.04–1.1
Anthropogenic sources: combustion (2010)	5,000 Mo/Fe	This study	11 [11–22] (49)	0.75–5.7
Braking (2010)	500 Mo/PM	This study	0.47 [0.47–4.7] (85)	
Agricultural dust	2–5 Mo/agricultural dust	Table S3	2.8 [2.8–7.1] (1)	

Note. The numbers in brackets represent the range of values, while in the parentheses in global source represent the percent (%) of the aerosols which are in the fine mode (PM$_{2.5}$).

emission, transport and deposition were all prognostic, varied with each time step, and included seasonality (Kok et al., 2014b). We estimated Mo emissions from desert dust to be 6.8 Gg Mo yr^{-1}, but with a large range of 3.2–32 Gg Mo yr^{-1} due to the large uncertainty in both the dust budgets and the concentration of Mo in dust (Table 1).

2.2.2. Agricultural Dust

Land-use dust from agricultural lands could also be a source of Mo, as the concentrations of Mo in soils are likely enriched in agricultural lands from the addition of Mo and P fertilizer, which also contains Mo (Barron et al., 2009; Charter et al., 1995). Agricultural production and related changes to the hydrologic cycle have led to increased anthropogenic dust (e.g., Ginoux et al., 2012). Here we used data sets of crop fraction of agricultural land for the present day, from the Coupled Model Intercomparison Project Phase 5 (CMIP5) inventory, in order to identify the relevant regions and multiply by the estimates of desert dust generated using the same algorithm for natural lands described above (Hurtt et al., 2011). We approximated that land-use sources of dust were 25% of the total dust as estimated from satellites (Ginoux et al., 2012), and used the prognostic dust scheme for the source, transport and deposition of the agricultural dust as a separate tracer. The Mo concentration in agricultural sources of dust was assumed to be higher than in natural lands. We used 2 mg Mo kg^{-1} as the best estimate and 5 mg Mo kg^{-1} for the high estimate (Table 1; Table S2). We estimated agricultural dust emissions to be 2.8 Gg Mo yr^{-1}, with a high estimate of 7.1 Gg Mo yr^{-1}.

2.2.3. Sea-Spray Aerosols

Sea-spray aerosols are entrained in the atmosphere from the ocean surface under high wind or wave conditions (O'Dowd & de Leeuw, 2007). We used the same approach as Wong et al. (2020b) with CAM6. Briefly, we used a constant concentration of Mo in seawater and the existing sea-spray aerosol module (Liu et al., 2011) and a value of 0.29 mg Mo kg^{-1} of sea-spray aerosol (Table 1), assuming sea-spray aerosol Mo concentrations reflect that of seawater (Wong et al., 2020b). Sea-spray aerosols are prognostic in the model, based on wind speeds, sea-ice, and temperature relationships (Liu et al, 2011). Sea-spray aerosol emission estimates were 0.75 Gg Mo yr^{-1} and were assumed to be uncertain here (range 0.38–3.8 Gg Mo yr^{-1}; Table 1) due to the uncertainty in sea spray aerosol budgets (Mahowald et al., 2011).

2.2.4. Volcanoes

Volcanic aerosols can be important local sources from noneruptive volcanoes (Wong et al., 2020b). Eruptive volcanoes could also be important, however, no appropriate long-term data set is available, so we focused on noneruptive emissions using the same approach as Wong et al. (2020b) but with CAM6. Briefly, we used the Mo to sulfur (S) ratio to approximate volcanic Mo emissions, normalized to estimates of S emissions from volcanoes from gridded global data sets (Spiro et al., 1992) of nonerupting volcanoes, using a temporally constant rate. We used a mass-based ratio of 4×10^{-4} of Mo/S from Nriagu (1989) (Table 1). Noneruptive volcanic emissions were estimated to be 0.71 Gg Mo yr^{-1} with a range of 0.35–3.5 Gg Mo yr^{-1} (Table 1).

2.2.5. Primary Biogenic Particles

Primary biogenic particles or airborne particles from biological material such as bacteria, spores, fungi, viruses, algae, and pollen are not explicitly modeled in the default CAM6, but can be important for trace elements in aerosols such as P (Mahowald et al., 2008). Thus we included a simple temporally constant parameterization of primary biogenic particles following Brahney et al. (2015) by assuming a leaf area index dependent source. We tuned the global amount such that over the Amazon, primary biogenic particles represent ∼50% of the PM$_{10}$ concentrations, as consistent with observations (Graham et al., 2003). Following Nriagu (1989) we used a Mo emission factor of 1.0 mg Mo kg^{-1} of primary biogenic aerosols, slightly higher than the upper bound of Mo concentration measurements made from vegetation, which range from 0.02 to 0.45 mg Mo kg^{-1} (Table 1; Data Set S4). This emission factor gave us a global Mo source of 0.49 Gg Mo yr^{-1}, and we assumed a range of 0.25–2.5 Gg Mo yr^{-1} (Table 1).

2.2.6. Wildfires

Wildfires may also represent a source of Mo (Nriagu, 1989), and emission data sets based on satellite burned area or other proxies for black carbon (BC) are widely available (van der Werf et al., 2004; Van Marle et al., 2017). We used the Coupled Model Intercomparison Project wildfire data set as an annually averaged temporally constant source (CMIP6) (Van Marle et al., 2017). This data set includes both natural and deforestation fires, as well as human suppression of current wildfires, and thus includes some impacts from human activities. To convert from BC to Mo, we used an emission factor of 0.5 mg Mo kg^{-1} burned mass (Nriagu, 1989), divided by the emission factor of BC of ∼0.5 g kg^{-1} burned mass (Andreae & Merlet, 2001) to get a ratio of Mo/BC of 1,000 mg kg^{-1} (Table 1). We estimated wildfire sources to be 0.02 Gg Mo yr^{-1} with a range of 0.01–0.1 Gg Mo yr^{-1}.

2.2.7. Anthropogenic Combustion

To estimate anthropogenic emissions of Mo from combustion sources, we made a first estimate by using a Fe emission inventory and assumed co-occurrence of Mo with Fe, multiplying by an observed emissions ratio. In some studies, Mo was not detected (Machemer, 2004), and in others, the Mo/Fe ratio was as high as 0.1 (Ge et al., 2001) or as low as 0.0001 (Querol et al., 1995), indicating Mo occurrence and emissions from coal and smelting-related emissions can be highly variable. We multiplied a central and upper "high" Mo/Fe ratio of 0.005 and 0.01 to the updated Fe inventory for 2010 in Speciated Pollutant Emissions Wizard (SPEW) (Bond et al., 2004; Rathod et al., 2020). The Fe emissions in SPEW include coal, smelting, fuel oil, and wood combustion in the industrial, transport, and residential sectors globally. The central ratio is based on the averaged observed Mo/Fe ratio in coal combustion and smelting-related emissions in Meij (1994; 0.0025), Machado et al. (2006; 0.002), and Sylvestre et al. (2017; 0.008). We did not include fugitive emissions from Mo mining. Combustion emissions were assumed to be temporally constant and were about 11 Gg Mo yr^{-1} for the year 2010, with 95% coming from smelting and coal combustion. This source was large, but with a large uncertainty associated with the estimated "high" value (Table 1).

2.2.8. Vehicle Braking

Braking-related emissions are the dominant nonexhaust vehicle emissions, and can contribute up to 50% of PM_{10} and 12% of $PM_{2.5}$ emissions from vehicles (Bozlaker et al., 2014; Grigoratos & Martini, 2015; Harrison et al., 2012). Braking-related emissions come from brake pads and brake discs, whereby the latter can contribute up to 70% of the total braking-related emissions (Hulskotte et al., 2014). Brake discs are generally made up of 95% Fe, 2% silica (SiO_2), and about 0.2% Mo (Hulskotte et al., 2014), the rest being copper (Cu), aluminum (Al), and Zn. The Mo fraction in brake dust PM ranges between 5 and 740 mg Mo kg^{-1} (Grigoratos & Martini, 2014; Thorpe & Harrison, 2008). The size distribution of braking-related emissions are generally unimodal with mass median aerodynamic diameters between 1 and 4 μm (Grigoratos & Martini, 2014), with sizes generally dominated by diameters of about 0.3–2 μm. We multiplied $PM_{2.5}$ and $PM_{10-2.5}$ vehicular combustion-related PM emissions (in SPEW) by 0.5 to estimate total PM emissions by brake-wear. Then, we multiplied the 2010 breakwear emissions by a central estimate of 500 mg Mo kg^{-1} brake-wear PM and assumed the "high" anthropogenic upper bound to be about 10 times the central emissions based on the uncertainty (1.8–8 mg PM km^{-1} $vehicle^{-1}$) in brake-wear emission factors in Grigoratos and Martini (2014) and the Mo fraction in brake-wear PM. These emissions ranged between 0.47 and 4.7 Gg Mo yr^{-1} for the year 2010 (Table 1). While vehicles in general may emit Mo through other pathways (Das & Chellam, 2020), we did not include other vehicle emissions here.

2.3. Soil Mo Observations and Estimates

To estimate the relative importance of Mo deposition on soil turnover time, we constructed a best estimate map of soil Mo concentrations. Current estimates assume a crustal abundance of 1–2 mg Mo kg^{-1} (Rudnick & Gao, 2003; Taylor & McLennan, 1995). Using the Thomson Web of Science Core Collection on October 10, 2019 we searched for the keywords "Mo" and "soil" and found 137 studies that reported a Mo concentration in surface soils based on a total or near-total digestion (Data Set S3). If latitude and longitude were not reported, we identified the nearest coordinates based on the reported study location.

We used two methods to construct a Mo soil map. In the first method, we categorized available Mo data by soil type classification and extrapolated Mo concentrations by soil type using an approach similar to Scanza et al. (2015). Of the 137 studies, 68 provided soil classification information either in the United States Department of Agriculture (USDA) or the Food and Agriculture (FAO) taxonomic system, which we converted to the USDA classification. We assigned a median amount of Mo for each soil type then aggregated up to the 1° × 1° USDA-NRCS Global Soil Regions map based on a reclassification of the FAO-UNESCO Soil Map of the World (Batjes, 1997), and data on Mo within different USDA's soil taxonomy orders as compiled here (Data Set S3). The within soil order variability of Mo concentrations is similar to the between order soil variability (Table S1), so the estimated spatial distribution of Mo in soils using this method does not compare well against observations (Figure S1a). For some soil orders, only three studies per soil order were reported, leaving the method of extrapolation by soil order as highly uncertain. In the second method, we extrapolated Mo concentrations in soils geographically through kriging interpolation using longitude and latitude coordinates. Because this method is simply an extrapolation of the available data, it does compare well, by definition with available data (Figures S1c and S1d). Because of the limited data, we used both methods to estimate the Mo concentration in soils.

The turnover time of Mo in the soils due to atmospheric deposition, in years, was calculated as the ratio of the soil Mo estimated to 1 m depth in each grid cell divided by the deposition flux, as estimated in Section 2.2. Because soil Mo cannot be assumed to be in steady state, we estimate a "pseudo-turnover time," which allows us to examine the ecological relevance of atmospheric Mo to the soil Mo reservoir in units of years (Okin et al., 2004).

3. Results

We present several types of evidence of anthropogenic sources of Mo, starting with local gradients between urban and rural regions, and including references to compositional analysis of aerosol observations. We then show the spatial distributions of the in situ concentration observations, compared to modeling with

and without anthropogenic sources. Finally, we show the resulting deposition maps and calculate the turn-over times in soils.

3.1. Analysis of Specific Sites

First, to better understand the nature of the sources of atmospheric Mo, we considered a few data sets where data were collected from cities and in nearby rural areas. Data collected from the sites in Switzerland, where a substantial fraction of the observations were above the detection limit for Mo, suggested that there was a clear gradient in the spatial distribution of Mo with higher concentrations in the more urban areas (Figure 2a), along with higher PM in general (Gianini et al., 2012a, 2012b; Hueglin et al., 2005).

Second, compositional analysis on the observations across all sites in Switzerland (Hueglin et al., 2005) using the approach by Qu et al. (2020) indicated that Mo is typically found in urban aerosols (Figure S2). This approach removed the concentration of aerosols and focused on the first two principal components of the composition using a selected set of elements. The compositional results strongly suggest anthropogenic sources of Mo for both $PM_{2.5}$ and PM_{10}; Mo concentrations tended to be higher in urban PM and that the PM with higher Mo concentrations was also enriched in other typically urban aerosols components for both $PM_{2.5}$ and PM_{10}.

Similarly, we examined compositional differences between two sites in Cuba where samples were collected simultaneously at a rural and an urban site (Morera-Gómez et al., 2018). Despite both sites being located on the coast with high deposition from sea-spray aerosols and under the North African dust plume in a region with some of the largest atmospheric Mo deposition rates (Wong et al., 2020b), the urban area was characterized by a higher Mo concentration than the rural site. The urban area also had a higher mixing ratio of Mo in PM (concentration of Mo divided by the total mass of PM), suggesting a large anthropogenic influence (Figure 2b). This high Mo/PM ratio was presumably due to the large petrochemical industries in this region, including a cement plant fueled by petroleum-coke, an asphalt plant, a power plant fueled by heavy crude oil, and Cuba's largest oil refinery. Bottom ash from the latter two industries had high contents of Mo (720 and 114 mg Mo kg^{-1}, respectively; Alonso-Hernández et al., 2011). Detailed source apportionment studies suggested that much of the particulate Mo in this region was associated with road traffic (48%), combustion sources (22%), with some contribution from marine aerosols (16%) and either cement industry or dust (10%) (Morera-Gómez et al., 2018). The more substantial proportion of road traffic Mo can be attributed to older cars running on diesel, which often concentrates heavy metals (Morera-Gómez et al., 2020). We also found similar results across three sites in Spain (Hernández-Pellón & Fernández-Olmo, 2019), where bulk Mo deposition rates were also higher closer to a manganese alloy plant than in urban background sites.

Finally, a long-term (26 year) observational data set at one site in Northern Europe demonstrated that atmospheric Mo peaked in the 1990s (Figure S3 using data, from Laing et al. (2014a, 2014b). This anomalous peak was likely caused by an anthropogenic source of Mo, because neither an increase over time, BC concentration ($r = 0.03$; Figure S3), nor nonsea-salt sulphate (Laing et al., 2013) can explain the peak.

3.2. Spatial Distribution of Atmospheric Mo

Our synthesis of the available observations of Mo in PM_{10} demonstrated that there were elevated concentrations observed across industrialized regions, such as Europe and Asia (Figure 3a). When we compared the model simulations with observations, we found that simulations with anthropogenic sources (Figure 3) were better at explaining Mo observations than only simulating with natural sources (Figure 4). When only natural sources were included, concentrations of Mo in industrialized regions, especially in Europe, were underestimated by several orders of magnitude (Figures 3 and 4). In some regions, the simulated anthropogenic estimate of emissions using our "high" estimate was a better match to the available data, although in others the "high" case overestimated the concentrations (Figure 3c). Although these results are difficult to verify with the limited observational data, the model simulations suggest that there is substantially more Mo in the atmosphere in Europe and Asia than in North America, primarily because of the higher estimates
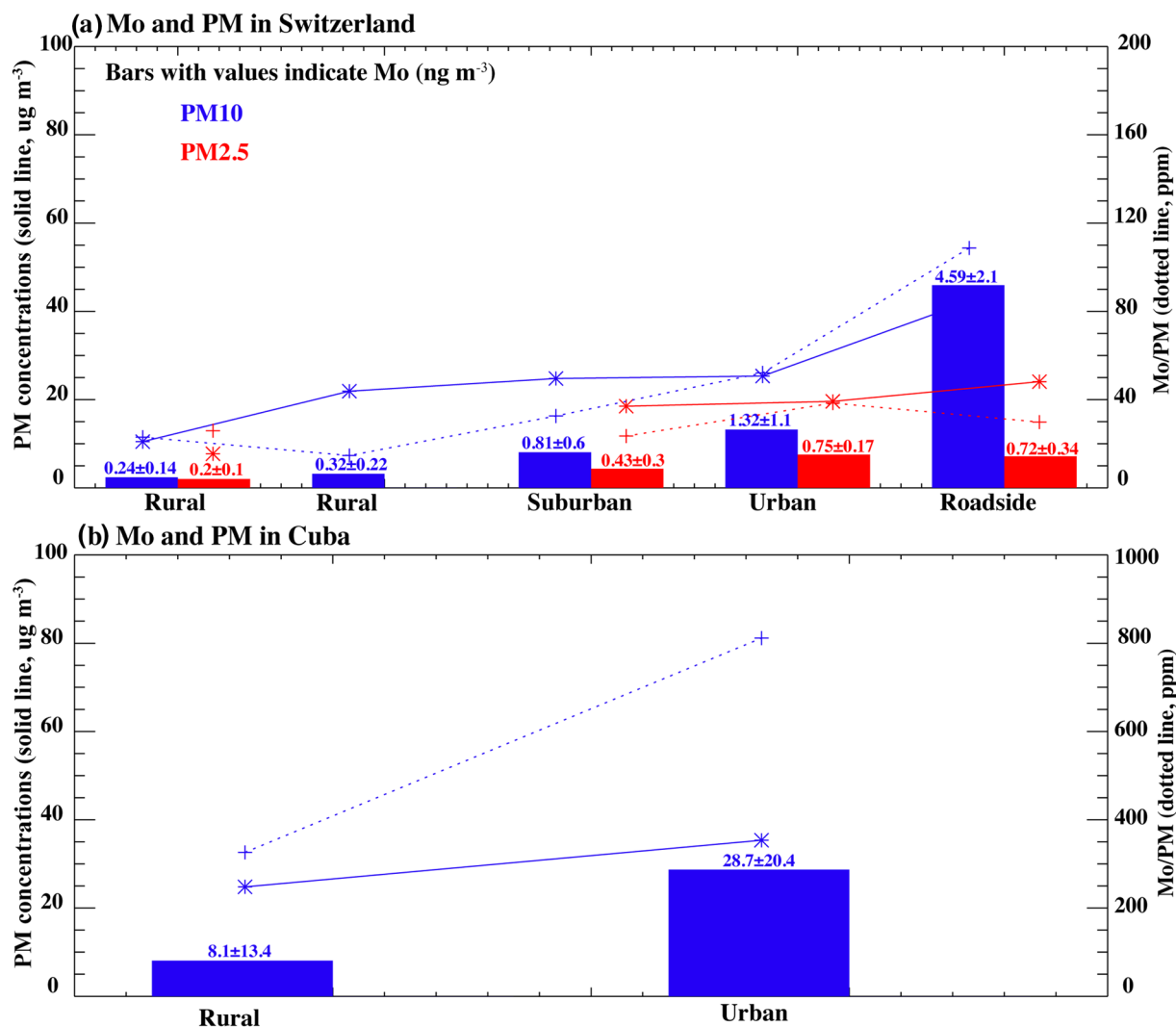
Figure 2. (a) Mo in particulate matter across Switzerland shown in the bars, with the values shown over each bar (ng m^{-3}) in blue (PM$_{10}$) and red (PM$_{2.5}$) increasing along a gradient toward more urbanized sites (left to right). Similarly, the total particulate matter increases in the more urban sites in both PM$_{10}$ (blue) and PM$_{2.5}$ (red) (solid line, μg m^{-3} left hand axis). The fraction of the Mo in PM tends to increase in more urban environments (dotted line, mg Mo kg^{-1}, right hand axis). Data are from Hueglin et al. (2005). (b) Similar for data from Cuba but only for PM$_{10}$. Note there is much more aerosol and Mo in Cuba than in Switzerland. Data are from Morera-Gómez et al., (2018). The means ± the standard deviations are presented for the Mo concentrations.

of combustion sources in these regions. While the model simulations did not correlate statistically significantly with the observations, they agreed on the same order of magnitude of Mo in the atmosphere.

Because the Mo concentration is typically low in atmospheric aerosols, we could have potentially biased our results by only including reported data where Mo was above the detection limit. To minimize bias, as discussed in the Methods section, if the reported values were below the detection limit, we approached the issue in two ways: first, if more than 50% of the observations at a particular site were above the detection limit, we included one-third of the minimum detection limit in the annual average. Second, the sites with less than 50% of observations above the detection limit provided information in that the limit of detection represented an upper bound on the Mo value, which we included as an upper bound in a secondary analysis (Figure 3d). However, including the upper bound did not appreciably change our picture of the Mo in the atmosphere (Figures 3d and 3c).

While a majority of modeled Mo was estimated to be in the PM$_{10}$ fraction due to the large desert dust, agricultural dust, and combustion sources, of which are 50%–99% in the coarse fraction (Table 1), we also
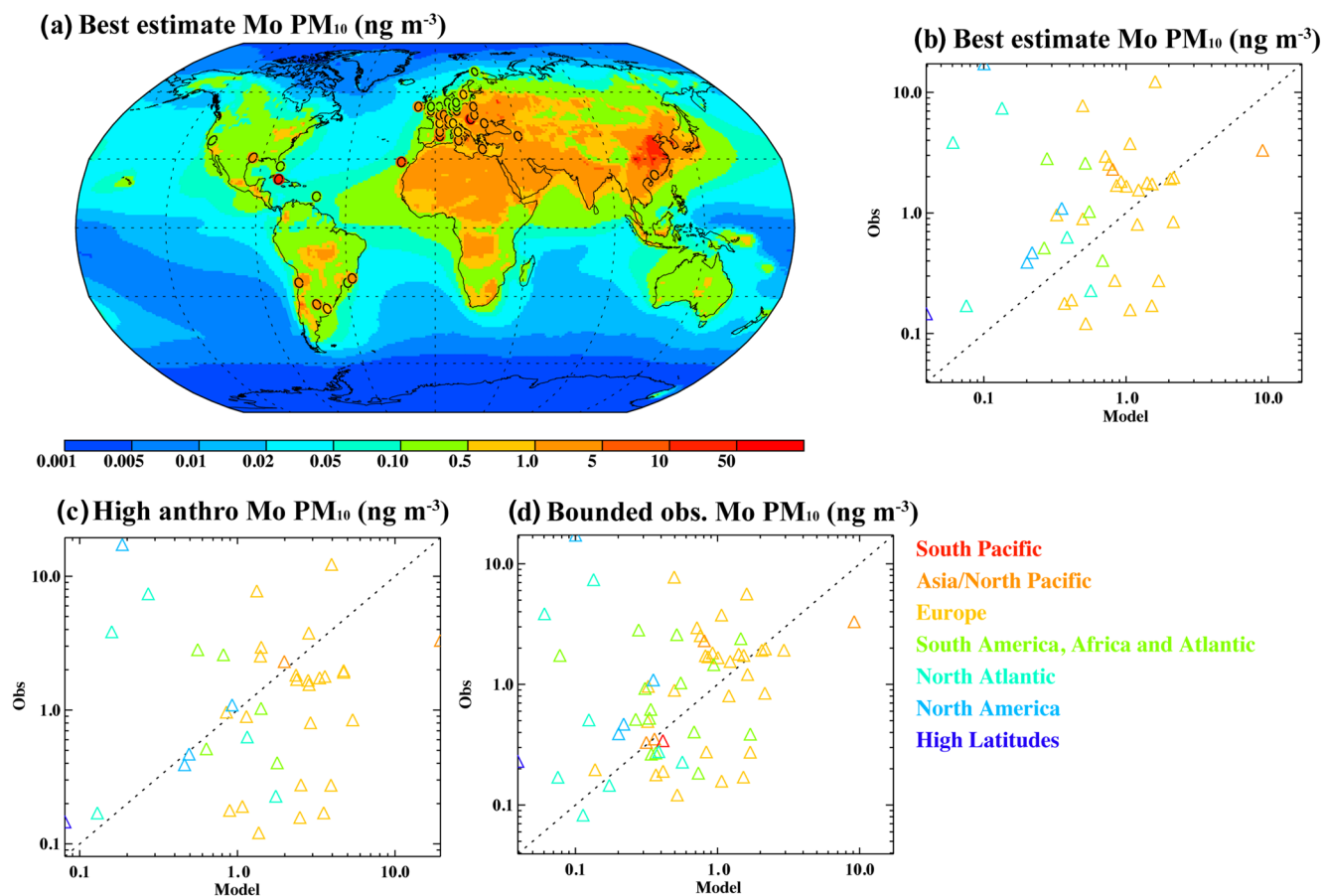
Figure 3. (a) Horizontal distribution of the surface concentrations of Mo (ng m^{-3}) in the PM$_{10}$ size fraction as simulated in the model using the best estimate scenario (contours) and from the observations (circles). Observations are averaged to a ~2° × 2° grid and compared to Community Atmosphere Model (CAM) (v6) results. (b) Scatterplot comparison of the modeled simulations in the best estimate scenario against observations (same as in a) ($n = 40$, $r = 0.01$). (c) Same as (b), except for the high anthropogenic model case ($n = 40$, $r = 0.00$). (d) Same as in (b), except that all stations are included, even if more than 50% of the observational values are below the detection limit to show the upper bound on observations as described in the Methods ($n = 61$, $r = 0.05$). In the scatter plots, colors indicate locations: South Pacific (red), Asia/North Pacific (orange), Europe (green), South America, Africa and Atlantic (cyan), North Atlantic (medium blue), North America (dark blue), and high latitudes (purple).

considered the distribution of Mo in the fine (PM$_{2.5}$) aerosol fraction. Similar to the PM$_{10}$ Mo fraction, observations of fine aerosol Mo also showed the highest values across industrialized regions (Figure 5a) and the simulations with only the natural sources were much lower than the observations (Figure S4). Similar to PM$_{10}$, assuming that the anthropogenic emissions are on the "high" end, the model matched the observations well in some places, such as some sites in Europe, Asia, and the North Pacific, while the model overpredicted in other sites (Figures 5b and 5c). We also compared the modeled concentrations of PM$_{2.5}$ to the upper bound in the concentrations where we included stations for which more than 50% of the data were below the detection limit (Figure 5d). There were many more sites that measured but did not detect Mo in the PM$_{2.5}$ fraction, especially in the US, so the scatter plot shows many more measurements than the PM$_{2.5}$ observations of detected Mo (Figures 5d and 5b). These comparisons showed that the modeled Mo was below the upper bound in most locations (Figure 5d).

When we compared total/bulk deposition observations to our model results (Figure S5), we also found strong evidence of anthropogenic Mo sources, as our model still underestimated deposition observations at half the sites (Figure S5). An error source likely arises from missing Mo-source aerosols with an aerodynamic diameter greater than the cutoff size of 10 μm by the model. Models begin to underestimate dust aerosols compared to observations at a diameter greater than approximately 5 μm (Adebiyi & Kok, 2020; Kok et al., 2017; Mahowald et al., 2014). This failure to capture large particles and their
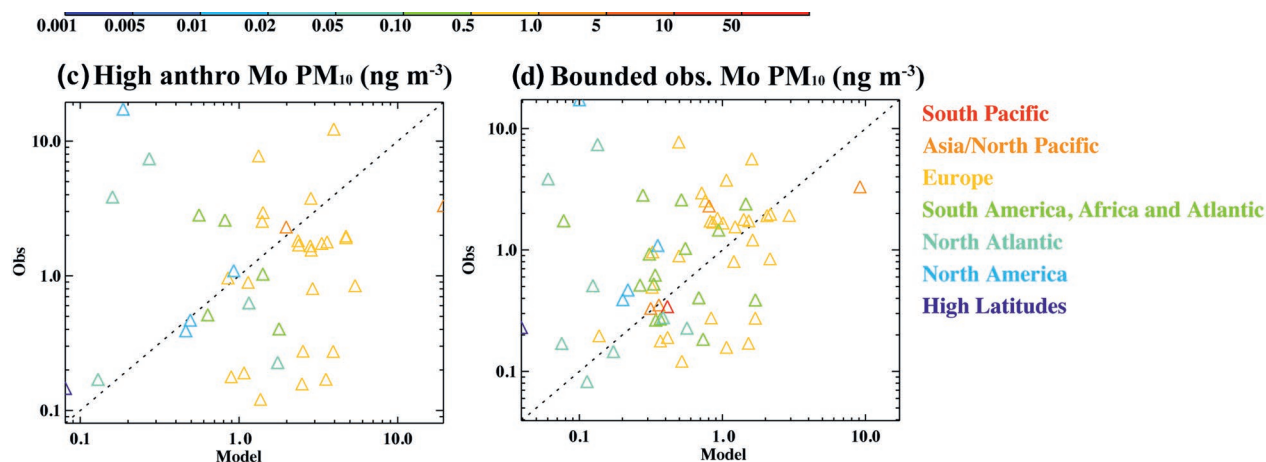
Figure 4. (a) Spatial distribution of the surface concentrations of Mo (ng m^{-3}) as simulated in the Community Atmosphere Model (CAM) (v6) using only natural sources (contours) overlain by observational data (circles). Observations are averaged to a ~2° × 2° grid and compared to the model. (b) Scatterplot comparison of the modeled surface concentrations of Mo (ng m^{-3}) in the natural sources only scenario against observations (same as in (a)) (n = 40, r = 0.13). In the scatter plots, colors indicate locations: South Pacific (red), Asia/North Pacific (orange), Europe (green), South America, Africa and Atlantic (cyan), North Atlantic (medium blue), North America (dark blue), and high latitudes (purple).

transport, which may dominate the deposition close to the source areas, by the model may also explain the model-observation discrepancy.

3.3. Sources of Atmospheric Mo

Modeled Mo deposition rates ranged over three orders of magnitude, from 1 to 5,000 μg m^{-2} yr^{-1}. From our spatially explicit model, we estimated that 8.77 Gg Mo yr^{-1} was emitted from natural sources with a range of 4.4–44 Gg Mo yr^{-1}, while 14.3 Gg Mo yr^{-1} was emitted from anthropogenic sources with a range of 14–34 Gg Mo yr^{-1} (Table 1). These results suggest that between 40% and 75% (best estimate: 62%) of the atmospheric Mo sources were anthropogenic. There are large uncertainties in natural sources of aerosols such as sea spray and dust, where estimates (dust: 6.6 Gg Mo yr^{-1}; sea-salt aerosols: 0.75 Gg Mo yr^{-1}; volcanic aerosols: 0.71 Gg Mo yr^{-1}) are different than those from Wong et al., (2020b) (dust: 4.3 Gg Mo yr^{-1}; sea-salt aerosols: 1.6 Gg Mo yr^{-1}; volcanic aerosols: 0.22 Gg Mo yr^{-1}) due to the difference in the models used. These model discrepancies are consistent with the large uncertainties in the amount and composition of natural aerosols in general (e.g., Mahowald et al., 2011). In the case of Fe, the differences between the modeled and observed aerosol concentrations were higher in areas where the natural aerosols are the dominant source (Rathod et al., 2020).

The estimated distribution of deposition for both the current best estimate (Figure 6a) and natural sources (Figure 6b) shows that while desert dust regions are the strongest natural sources and have the largest deposition rates, there is also intense deposition in industrialized regions. The ratio of current anthropogenic to natural sources of Mo in the model suggests that there is a large perturbation (up to 100X higher) on Mo deposition rates in many regions in both the best estimate and the "high" anthropogenic case (Figures 6c and 6d). When we examine the relative contribution of sources to total Mo deposition across regions (Figure 7), we found that desert dust deposition dominated close to the main dust source areas and sea-spray aerosols over the oceans (Wong et al., 2020b), anthropogenic combustion sources dominated in industrialized regions, and agricultural dust dominated in cultivated areas (Figure 7, Table 1).

Natural sources of Mo from terrestrial regions such as primary biogenic particles and wildfires can remove Mo from ecosystems (Kauffman et al., 1995; Mahowald et al., 2005). For example, we estimated that in the Amazon (290°E-320°E, 15°S-0°N) wildfire aerosols deposit 0.18 Gg Mo yr^{-1} and cause the release of 0.20 Gg Mo yr^{-1}, while primary biogenic particles deposit 0.048 Gg Mo yr^{-1} and release 0.052 Gg Mo yr^{-1}. Thus, although most Mo is locally "recycled" within ecosystems, we estimate that within this grid cell, about 10%
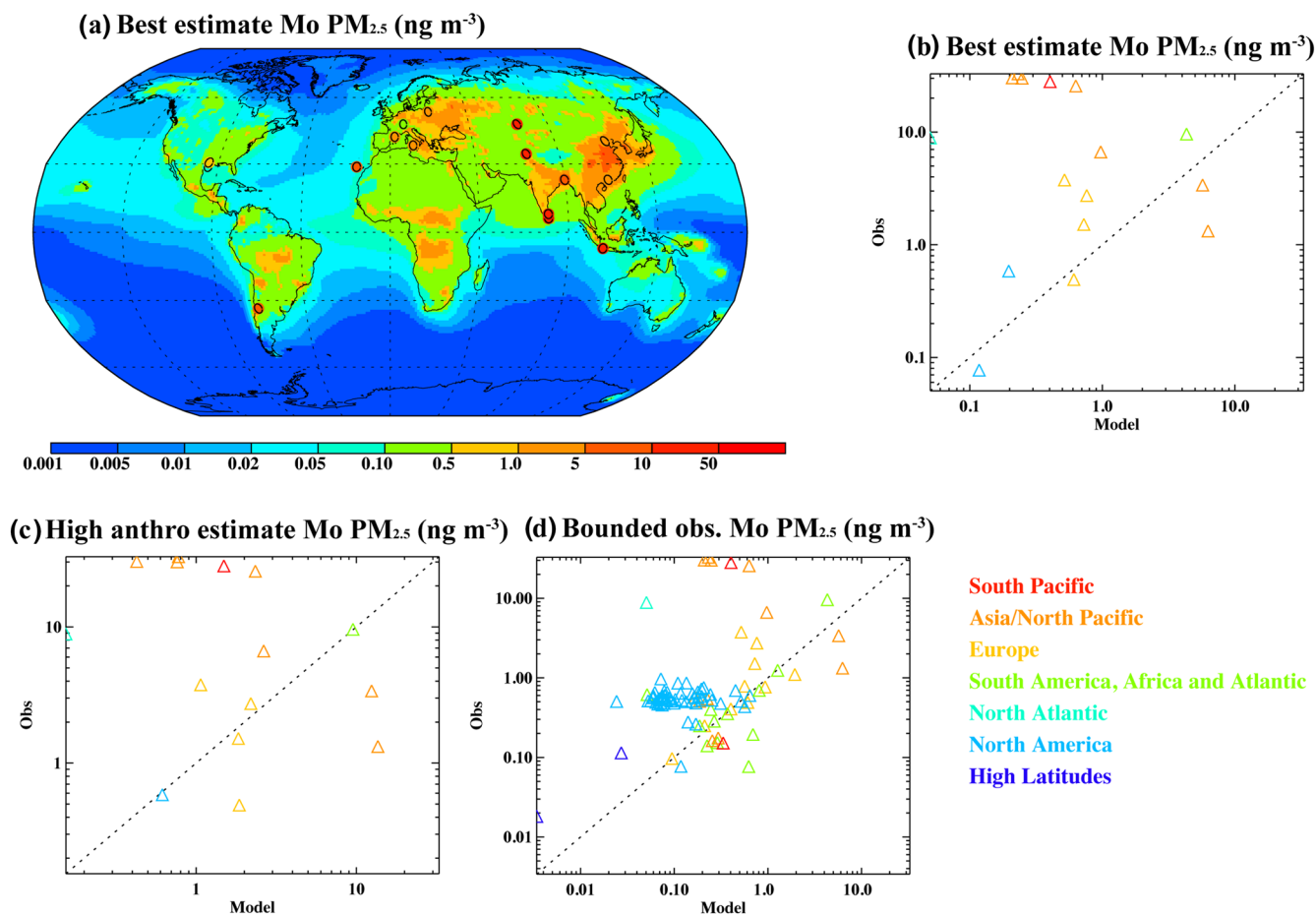
(a) Best estimate Mo PM₂.₅ (ng m⁻³)

(b) Best estimate Mo PM₂.₅ (ng m⁻³)

(c) High anthro estimate Mo PM₂.₅ (ng m⁻³) **(d) Bounded obs. Mo PM₂.₅ (ng m⁻³)**

South Pacific
Asia/North Pacific
Europe
South America, Africa and Atlantic
North Atlantic
North America
High Latitudes

Figure 5. (a) Same as Figure 3, but for PM₂.₅. Spatial distribution of the surface concentrations PM₂.₅ of Mo (ng m⁻³) as simulated in the Community Atmosphere Model (CAM) (v6) using the best estimate scenario (contours) and overlain by observational data (circles). Observations are averaged to a ~2° × 2° grid and compared to the model. (b) Scatterplot comparison of the modeled surface concentrations PM₂.₅ of Mo (ng m⁻³) in the best estimate scenario against observations (same as in a) ($n = 16$, $r = -0.32$). (c) Same as (b), except for the high anthropogenic model case ($n = 16$, $r = -0.13$). (d) Same as in (b), except that all observational values below the detection limit as included to show the upper bound on observations as described in the Methods ($n = 93$, $r = 0.07$). In the scatter plots, colors indicate locations: South Pacific (red), Asia/North Pacific (orange), Europe (green), South America, Africa and Atlantic (cyan), North Atlantic (medium blue), North America (dark blue), and high latitudes (purple).

of Mo from wildfires and primary biogenic particles escapes into the ocean each year, which over geological time could result in a deficit. However, Mo in this grid cell is estimated to be replaced by long-range transported sea-spray aerosol Mo (0.003 Gg Mo yr⁻¹) and desert dust Mo (0.01 Gg Mo yr⁻¹), and has been enhanced by anthropogenic sources of Mo, especially combustion (0.08 Gg Mo yr⁻¹).

3.4. Implications for Changes in Soil Mo Turnover Times

To assess the relative impact of aerosol deposition on soil Mo, we estimated turnover times across the top 1 m of soil, which reflects the importance of aerosol Mo inputs relative to the modern soil Mo reservoir (Okin et al., 2004). Using two approaches of approximating Mo soil concentrations (see Methods 2.3), we found that soil Mo turnover times vary between 1,000 years at the shortest (in regions where desert dust is the dominant source for Mo) up to millions of years (Figure 8). Anthropogenic sources shorten turnover times (0.01X) regardless of the interpolation method for soil Mo because of the strong increase in Mo in industrialized regions.

These results suggest that Mo deposition from anthropogenic sources could perturb and accelerate Mo turnover in some regions if anthropogenic activity continues at the same rate into the future. However, these
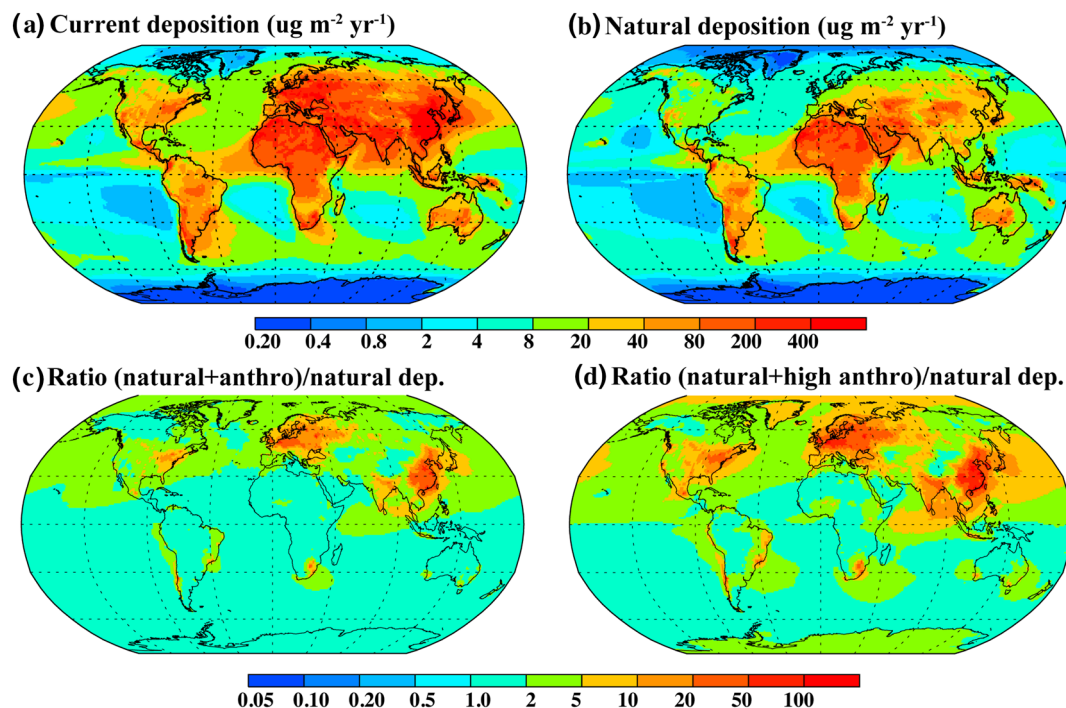
Figure 6. Spatial map of modeled deposition in the Community Atmosphere Model (CAM) (v6) results in the current climate of Mo in PM_{10} aerosols ($\mu g\ m^{-2}\ yr^{-1}$) for (a) the current (natural and anthropogenic) climate best estimate and (b) with natural sources only. The ratio of natural to total Mo deposition are displayed as (c) the ratio of Mo deposition in the current climate (natural and best estimate anthropogenic) over natural deposition and (d) the ratio of Mo deposition in the current climate with the "high" anthropogenic estimate case (natural and high anthropogenic) over natural deposition.

turnover times are still long (1,000 years or more) compared to other perturbations, such as deforestation or biomass burning (Andela et al., 2017; Hansen et al., 2013), which have accelerated turnover times for P in biomass from 64 to 50 years in regions of the Amazon (Mahowald et al., 2005).

4. Discussion

Our models and synthesis of observations suggest that anthropogenic activity has substantially altered the atmospheric Mo cycle and are accelerating Mo turnover rates in soils. From modeling emissions of Mo, we estimated that anthropogenic sources, 1 (14–34) Gg Mo yr^{-1} (range in brackets), are likely to be equal to or exceed the natural sources, which we estimated to be 8.8 (4.4–44) Gg Mo yr^{-1} (Table 1). Even when we included anthropogenic sources in our model, observations of Mo sometimes exceeded modeled estimates, suggesting that the model simulations may be underpredicting deposition in some regions. In areas with strong influence from industrialization, fires, and agricultural land-use change, these activities have likely altered Mo cycles by a factor of 2 or more (Figure 7). Anthropogenic perturbation of the Mo cycle is on the same order of magnitude as the alteration of other metals such Al, V, mercury (Hg), and lead (Pb) (Rauch & Pacyna, 2009; Schlesinger et al., 2017; Selin, 2009; Sen & Peucker-Ehrenbrink, 2012).

4.1. Sources of Discrepancy Between the Model and Observational Data

Differences between the model and the observations could be due to our model only predicting source emissions, but not resuspension of particles that are captured by observations. For example, direct emissions from vehicle braking were included in the model, but atmospheric sources such as road dust resuspension,
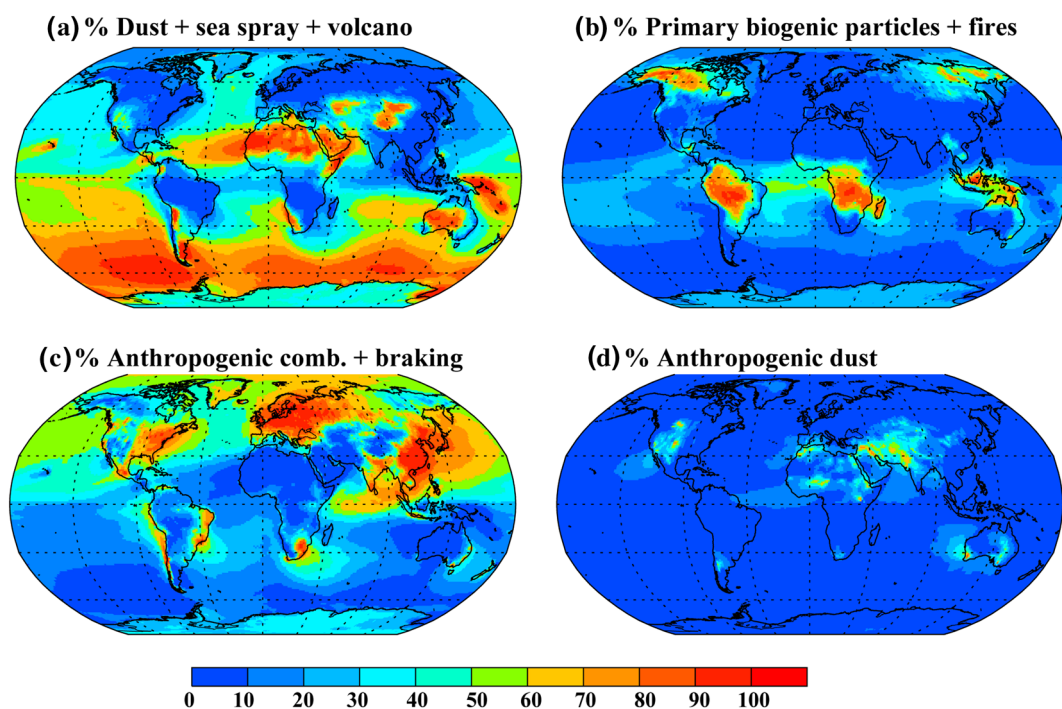
Figure 7. Percentage of Mo deposition in the best estimate case in the current climate from different sources in the Community Atmosphere Model (CAM) (v6): (a) natural desert dust, sea-spray aerosols, and volcanoes, (b) primary biogenic particles (PBP) and wildfires from natural ecosystems, (c) anthropogenic combustion and braking emissions, and (d) anthropogenic land use and agricultural dust.

which can comprise up to 50% of PM_{10} and a quarter of $PM_{2.5}$ (Bozlaker et al., 2014), were not included. Thus resuspension of sources to the atmosphere may have contributed to the model underestimation in some regions with higher densities of industrialization.

In addition to resuspension of particles, model underprediction in some regions could also be from unaccounted sources that were not included in the model, such as fugitive mining, PM emitted from vehicle exhaust, and other nonexhaust sources of vehicle Mo. Direct vehicle exhaust sources include engine wear (Gonet & Maher, 2019) and catalytic converters (Dillner et al., 2005). Detailed analysis of sites in the region of Rio de Janeiro demonstrated that the largest source of Mo in PM_{10} came from catalytic converters (da Silva et al., 2008) due to the rising usage of $Pd-Mo/Al_2O_3$ catalysts in Brazil (De Mello et al., 2003; Schmal et al., 1999), which we were unable to include in our model. While we considered vehicle braking emissions based on correlations with Fe, we did not account for other nonexhaust related emissions, such as lubricants, where Mo sulfides are often added (Amato et al., 2010) and can compose between 5% and 29% of brake lining (Thorpe & Harrison, 2008).

4.2. Mass Balance of Mo Deposition with Riverine Exports

Comparing annual Mo riverine export to total deposition estimates from our model also suggests anthropogenic perturbation of the Mo cycle. From our synthesis of Mo in riverine samples (Data Set S5), we estimated that around 21 Gg Mo yr^{-1} moved from terrestrial ecosystems through rivers to oceans every year, based on a median Mo river concentration of 0.56 μg Mo L^{-1} (Data Set S5) and an annual discharge of 37,288 km^3 yr^{-1} (Dai & Trenberth, 2002). The riverine estimate of 21 Gg yr^{-1} fell close to our median atmospheric deposition estimate of 23 Gg Mo yr^{-1} (Table 1). However, the riverine export fluxes typically only represent export from terrestrial ecosystems, while our deposition estimates represent global fluxes to land and oceans. Thus, the large riverine estimates relative to our modeled estimates also suggest significant anthropogenic inputs. Our riverine Mo also exceeds the previous estimate of 17.3 Gg Mo yr^{-1} from the late 1970s (Martin

(a) Current dep./USDA soil map

(b) Current dep./interpolated soil map

(c) Natural dep./USDA soil map

(d) Natural dep./interpolated soil map

1.0 2 4 10 20 40 100 200 400 1000 2000
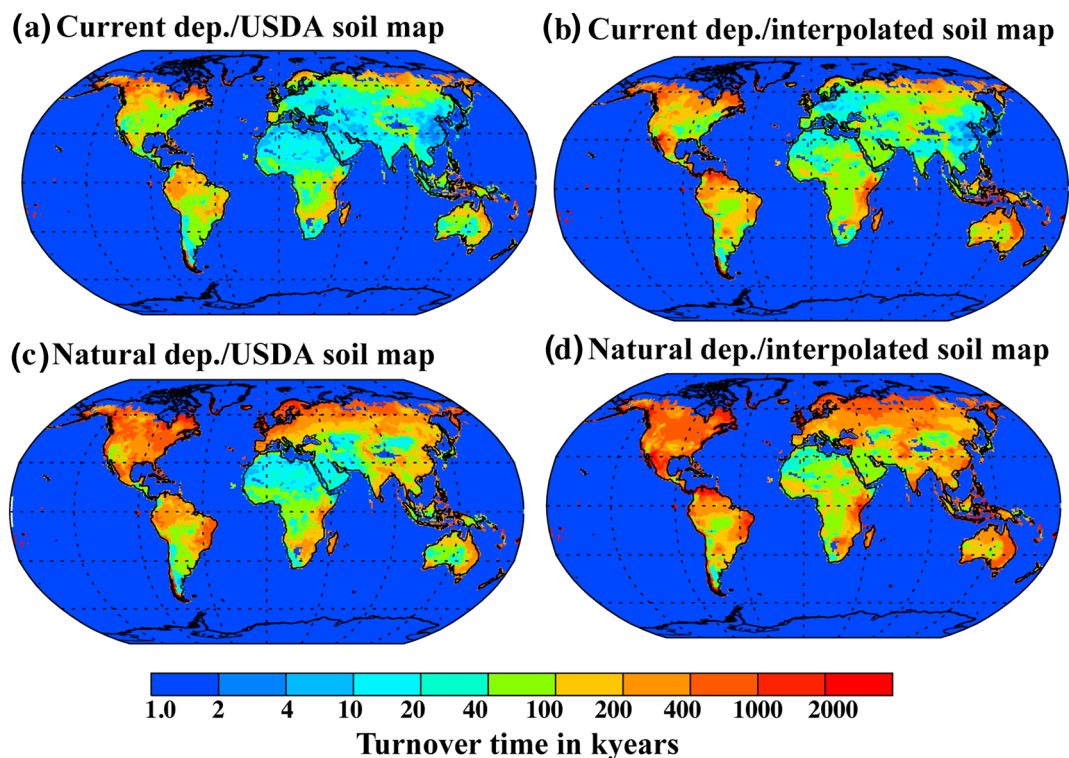
Turnover time in kyears

Figure 8. Turnover time (kiloyears) of soil Mo from current (natural plus anthropogenic) deposition in the Community Atmosphere Model (CAM) (v6) in the current climate calculated by (a) the median Mo amounts in USDA soil orders (Table S1; Data Set S3) and (b) and using kriging interpolation, and turnover time of soil Mo from natural deposition only calculated by the median Mo amounts in USDA soil orders (Table S1; Data Set S3) (c and d) and using kriging interpolation. Turnover time is estimated as the amount of Mo in the top meter of soil over the deposition flux calculated in the model for the current and natural cases.

& Meybeck, 1979) but falls below the recent estimate of 36 Gg Mo yr^{-1} (Sen & Peucker-Ehrenbrink, 2012), which implies that our riverine estimates of Mo are relatively conservative.

4.3. Impacts of Anthropogenic Mo Deposition on N Cycling

Human perturbation of the Mo cycle is likely relieving Mo limitation on N fixation in regions isolated from strong N deposition. First, anthropogenic sources of Mo likely have stronger effects on N cycling relative to natural sources, as anthropogenic sources are typically more soluble (Desboeufs et al., 2005). Second, Mo as a constraint on N fixation is seemingly widespread across many terrestrial ecosystems (Dynarski & Houlton, 2018), and in N-limited areas, increased Mo deposition may facilitate higher rates of N fixation. As discussed by Wong et al. (2020b), experimental addition rates of 39 µg Mo m^{-2} yr^{-1} have been found to stimulate free-living N fixation on a tropical forest floor (Barron et al., 2009), well within the estimated annual rates of current total Mo deposition (8–80 µg Mo m^{-2} yr^{-1} across many ecosystems (Figure 6). While Mo was added in a soluble, bioavailable form in the experiments of Barron et al., (2009), we present these rates as an example for the scale at which increases in Mo availability can impact N fixation, particularly over decades as deposition accumulates in the ecosystem. Third, in areas with Mo limitation, such as regions that are isolated from low external inputs of Mo with leaf litter concentrations less than 200–300 ng Mo g^{-1} leaf litter (Darnajoux et al., 2019; Reed et al., 2013), alternative nitrogenases may play an important role (Darnajoux et al., 2017; Zhang et al., 2016). Genes encoding alternative nitrogenases have been found in a variety of terrestrial ecosystems (Betancourt et al., 2008). Anthropogenic perturbation of the Mo cycle may shift alternative nitrogenase activity toward the more common and preferred Mo-based form of nitrogenase (Eady, 1996). Darnajoux et al. (2019) sampled across a gradient of atmospheric metal deposition in a north-

eastern American boreal forest and found an inverse correlation between high Mo deposition, indicated by Mo contents in lichens, and alternative vanadium-based nitrogenase activity. These results suggest that increased anthropogenic Mo deposition in previously pristine ecosystems that received little to no natural Mo or N deposition may enhance N fixation.

Terrestrial regions where Mo limitation have been found, which include several temperate, tropical, and boreal ecosystems (Dynarski & Houlton, 2018; Wong et al., 2020b; and references therein), may be particularly sensitive to anthropogenic Mo inputs. Other regions that may be similarly sensitive to anthropogenic perturbations of the Mo cycle are regions where N limitation is strong and new inputs of Mo from weathering or natural atmospheric deposition are low. These areas include North American boreal forests, which may be affected by tar sands (Robertson et al., 2019), recovering Neotropical tropical forests (Batterman et al., 2013; Davidson et al., 2007) and savannas, which may be affected by biomass burning and agricultural dust, and recovering Asian tropical forests, which may be affected by combustion.

As temperatures and CO_2 concentrations increase and precipitation patterns change, the demand for N and thus increased N fixation may increase and exacerbate Mo limitation (Hungate et al., 2004; Zheng et al., 2020) in regions isolated from increasing N deposition inputs. While Mo limitation has been found across a few ecosystems, these studies have been concentrated in certain regions (Dynarski & Houlton, 2018). Before we can fully understand or predict how anthropogenic Mo may be affecting the N cycle, future research should focus on where and when Mo is limiting and contextualize Mo limitation with C, N, and P availability (Wong et al., 2020a; Wurzburger et al., 2012; Zheng et al., 2018).

Ultimately, the influence that anthropogenic Mo inputs will have on ecosystem function depends on the stoichiometry of other elemental inputs, such as N and P, and the nutrient status of the ecosystem being impacted (Figure 9). The signature of N deposition across the global is large, and anthropogenic N inputs will likely continue to increase in the future (Peñuelas et al., 2012, 2013). In these regions where anthropogenic N deposition inputs are large, stimulation of N fixation from increased atmospheric Mo may be offset (Bauters et al., 2018; Dentener et al., 2006). When examining Mo deposition together with N and P deposition, the largest sources of anthropogenic Mo tend to co-occur with the highest rates of N deposition, and the largest sources of natural Mo co-occur with the largest sources of atmospheric P (Figures 9a and 9b). Regions that receive low rates of N deposition and high rates of P deposition (or a lower N:P ratio) will likely be more sensitive to Mo as relieving P limitation would shift the ecosystem toward N limitation where increased Mo is advantageous. Other regions where Mo deposition may impact ecosystem function are regions where anthropogenic activity has accelerated Mo cycling to a greater extent than N and P cycling alone in many terrestrial ecosystems, as evidenced by the decrease in current to preindustrial N:Mo and P:Mo ratios in many temperate, boreal, and tropical regions (Figures 9c and 9d).

The large increase in atmospheric Mo will likely increase the imbalance between N and P globally, as anthropogenic N inputs have greatly exceeded P inputs (Peñuelas et al., 2012, 2013). In addition to the role of Mo in N fixation, Mo is essential for dissimilatory nitrate reduction, reducing nitrate to nitrite, often a rate-limiting step in N assimilation (Begara-Morales et al., 2020). Relieving any Mo constraints on the N cycle will contribute to increasing P limitation in both natural and agricultural ecosystems, which could impact ecosystems with effects ranging from changing stoichiometry, species composition, and genomic composition (Peñuelas et al., 2012). The increased imbalance between the N and P cycles, and therefore ecological impact, may be greatest in the Northern Hemisphere, where both current to preindustrial N and Mo deposition are the highest (Figure 9e).

4.4. Limitations of the Observational Data and Model

This paper represents a first attempt to constrain the spatial distribution of anthropogenic sources such as from combustion, braking, and land use. Most of the observations presented here were located in industrialized countries. To better understand the atmospheric contribution to the Mo cycle, more observations of concentrations and deposition are required. In addition, we also need a better understanding of the sources of Mo. For example, we used a recent Fe emission compilation as a baseline for Mo from combustion (as most Mo co-occurs with Fe), however more in-depth consideration of Mo and other ecologically important
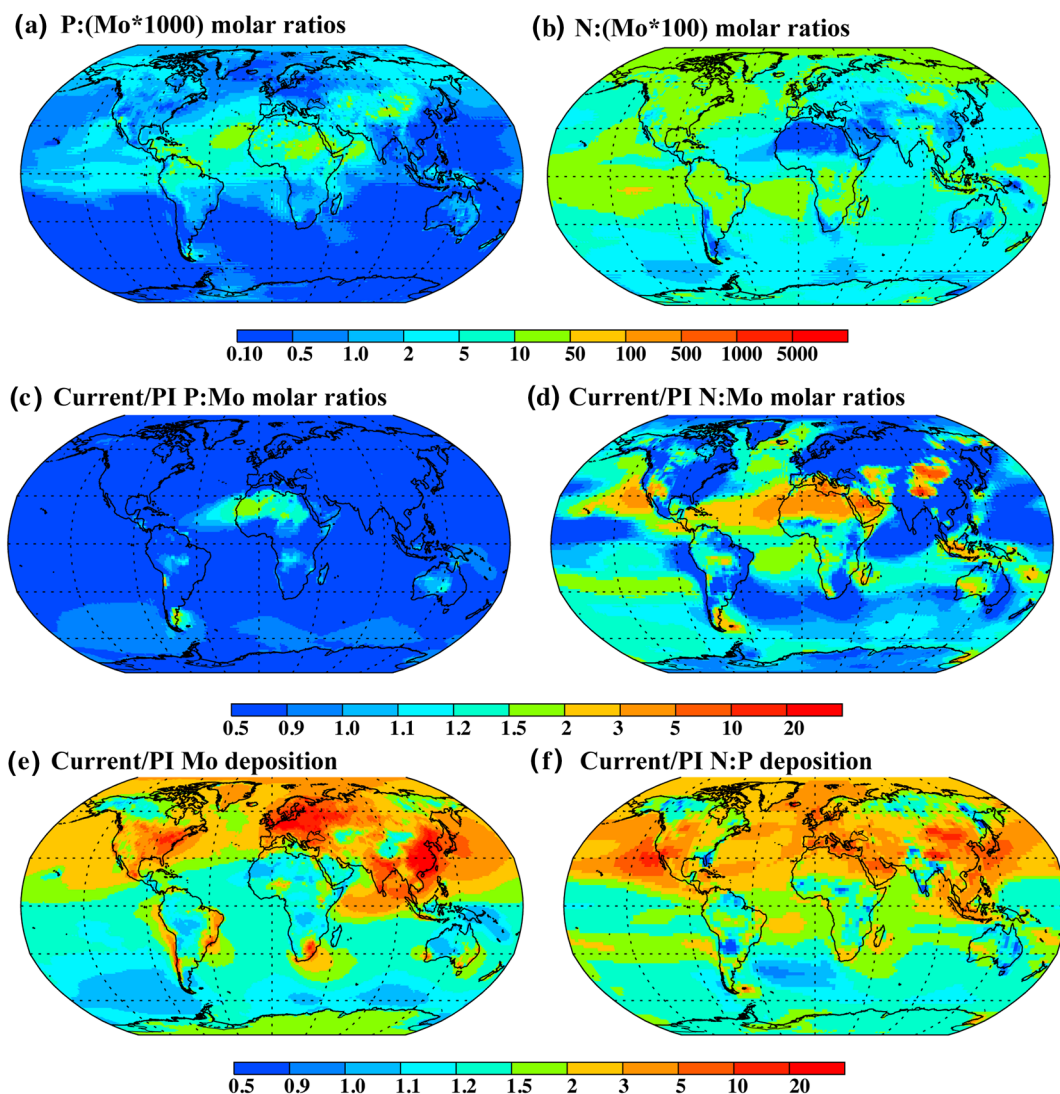
Figure 9. Spatial distribution of current (natural plus anthropogenic) modeled atmospheric deposition of (a) P:(Mo*1,000) and (b) N:(Mo*100) molar ratios. (c) Ratios of current to preindustrial P:Mo, (d) N:No, (e) Mo only, and (f) N:P atmospheric deposition in the Community Atmosphere Model (CAM) (v6). Current and preindustrial estimates of atmospheric N and P deposition are derived from the same methodology as described in Brahney et al. (2015).

metals, especially from mining and smelting (Rathod et al., 2020) would improve estimates. Finally, constraining emission factors from natural sources as well as from vehicle emission processes will improve our estimates of modeled Mo in remote as well as industrial and urban areas (Das & Chellam, 2020).

5. Conclusions

Low Mo availability can constrain N fixation and uptake in some terrestrial and aquatic ecosystems. Atmospheric deposition of Mo is likely an important source of Mo in N-limited terrestrial ecosystems with highly weathered soils, and previous studies have suggested substantial anthropogenic perturbation to Mo at the global level and from local observations. We explored, for the first time, the spatial distribution of current atmospheric Mo, and estimate from a combination of observations and modeling that about two-thirds of current atmospheric Mo sources are from anthropogenic sources (14.3 Gg Mo yr^{-1}) compared to natural sources (8.77 Gg Mo yr^{-1}). In industrialized regions, deposition may have increased by 100X or more from

combustion of coal and smelting operations. There are large uncertainties in these estimates, suggesting that anthropogenic sources represent between 40% and 75% of the total sources of Mo. Our modeling of Mo deposition did not capture the spatial distribution of either PM_{10} or $PM_{2.5}$, so future studies could improve the simulations and refine the role of mining and smelting, especially as the energy transition to renewables is likely to require more Mo and other metals. However, given the low concentrations of Mo in the atmosphere and the limited understanding of Mo sources, this study represents an important step forward in understanding Mo cycling. The substantial changes in Mo deposition from human activity is likely accelerating increase N cycling across ecosystems.

Data Availability Statement

Observational synthesis available in the supplemental materials, while model results are available at the Cornell eCommons repository (https://doi.org/10.7298/nzhv-4579).

References

Adebiyi, A. A., & Kok, J. F. (2020). Climate models miss most of the coarse dust in the atmosphere. *Science Advances*, *6*(15), 1–10. https://doi.org/10.1126/sciadv.aaz9507

Alastuey, A., Querol, X., Aas, W., Lucarelli, F., Pérez, N., Moreno, T., et al. (2016). Geochemistry of PM_{10} over Europe during the EMEP intensive measurement periods in summer 2012 and winter 2013. *Atmospheric Chemistry and Physics*, *16*(10), 6107–6129. https://doi.org/10.5194/acp-16-6107-2016

Albani, S., Mahowald, N., Perry, A., Scanza, R., Zender, C., & Flanner, M. G. (2014). Improved representation of dust size and optics in the CESM. *Journal of Advances in Modeling Earth Systems*, *6*(3), 541–570. https://doi.org/10.1002/2013MS000279

Alonso-Hernández, C. M., Bernal-Castillo, J., Bolanos-Alvarez, Y., Gómez-Batista, M., & Diaz-Asencio, M. (2011). Heavy metal content of bottom ashes from a fuel oil power plant and oil refinery in Cuba. *Fuel*, *90*(8), 2820–2823. https://doi.org/10.1016/j.fuel.2011.03.014

Alves, C. A., Gomes, J., Nunes, T., Duarte, M., Calvo, A., Custódio, D., et al. (2015). Size-segregated particulate matter and gaseous emissions from motor vehicles in a road tunnel. *Atmospheric Research*, *153*, 134–144. https://doi.org/10.1016/j.atmosres.2014.08.002

Amato, F., Moreno, T., Pandolfi, M., Querol, X., Alastuey, A., Delgado, A., et al. (2010). Concentrations, sources and geochemistry of airborne particulate matter at a major European airport. *Journal of Environmental Monitoring*, *12*(4), 854–862. https://doi.org/10.1039/b925439k

Andela, N., Morton, D. C., Giglio, L., Chen, Y., Van Der Werf, G. R., Kasibhatla, P. S., et al. (2017). A human-driven decline in global burned area. *Science*, *356*(6345), 1356–1362. https://doi.org/10.1126/science.aal4108

Andreae, M. O., & Merlet, P. (2001). Emission of trace gases and aerosols from biomass burning. *Global Biogeochemical Cycles*, *15*(4), 955–966. https://doi.org/10.5194/acp-11-4039-2011

Andreae, T. W. (2002). Light scattering by dust and anthropogenic aerosol at a remote site in the Negev desert, Israel. *Journal of Geophysical Research*, *107*(D2), 4008. https://doi.org/10.1029/2001JD900252

Atanacio, A. J., & Cohen, D. D. (2020). *The IAEA/RCA fine and coarse PMF receptor fingerprint database*, Sydney, Australia: Australian Nuclear Science and Technology Organisation. Retrieved from http://www.ansto.gov.au/aspdatabases

Barraza, F., Lambert, F., Jorquera, H., Villalobos, A. M., & Gallardo, L. (2017). Temporal evolution of main ambient PM 2. 5 sources in Santiago, Chile, from 1998 to 2012. *Atmospheric Chemistry and Physics*, *17*(16), 10093–10107. https://doi.org/10.5194/acp-17-10093-2017

Barron, A. R., Wurzburger, N., Bellenger, J. P., Wright, S. J., Kraepiel, A. M. L., & Hedin, L. O. (2009). Molybdenum limitation of asymbiotic nitrogen fixation in tropical forest soils. *Nature Geoscience*, *2*(1), 42–45. https://doi.org/10.1038/ngeo366

Batjes, N. H. (1997). A world dataset of derived soil properties by FAO-UNESCO soil unit for global modelling. *Soil Use and Management*, *13*(1), 9–16. https://doi.org/10.1111/j.1475-2743.1997.tb00550.x

Batterman, S. A., Hedin, L. O., Van Breugel, M., Ransijn, J., Craven, D. J., & Hall, J. S. (2013). Key role of symbiotic dinitrogen fixation in tropical forest secondary succession. *Nature*, *502*(7470), 224–227. https://doi.org/10.1038/nature12525

Bauters, M., Drake, T. W., Verbeeck, H., Bodé, S., Hervé-Fernández, P., Zito, P., et al. (2018). High fire-derived nitrogen deposition on central African forests. *Proceedings of the National Academy of Sciences of the United States of America*, *115*(3), 549–554. https://doi.org/10.1073/pnas.1714597115

Begara-Morales, J. C., Chaki, M., Valderrama, R., Mata-Pérez, C., Padilla-Serrano, M. N., & Barroso, J. B. (2020). Chapter 29 - Nitric oxide under abiotic stress conditions. *Plant Life Under Changing Environment*, 735–754. https://doi.org/10.1016/b978-0-12-818204-8.00032-1

Betancourt, D. A., Loveless, T. M., Brown, J. W., & Bishop, P. E. (2008). Characterization of diazotrophs containing Mo-independent nitrogenases, isolated from diverse natural environments. *Applied and Environmental Microbiology*, *74*(11), 3471–3480. https://doi.org/10.1128/AEM.02694-07

Bond, T. C., Streets, D. G., Yarber, K. F., Nelson, S. M., Woo, J.-H., & Klimont, Z. (2004). A technology-based global inventory of black and organic carbon emissions from combustion. *Journal of Geophysical Research*, *109*(D14), D14203, 1–43. https://doi.org/10.1029/2003JD003697

Boonpeng, C., Polyiam, W., Sriviboon, C., Sangiamdee, D., Watthana, S., Nimis, P. L., & Boonpragob, K. (2017). Airborne trace elements near a petrochemical industrial complex in Thailand assessed by the lichen *Parmotrema tinctorum* (Despr. ex Nyl.) Hale. *Environmental Science and Pollution Research*, *24*(13), 12393–12404. https://doi.org/10.1007/s11356-017-8893-9

Bozlaker, A., Buzcu-Güven, B., Fraser, M. P., & Chellam, S. (2013). Insights into PM_{10} sources in Houston, Texas: Role of petroleum refineries in enriching lanthanoid metals during episodic emission events. *Atmospheric Environment*, *69*, 109–117. https://doi.org/10.1016/j.atmosenv.2012.11.068

Bozlaker, A., Prospero, J. M., Price, J., & Chellam, S. (2019). Identifying and quantifying the impacts of Advected North African dust on the concentration and composition of airborne fine particulate matter in Houston and Galveston, Texas. *Journal of Geophysical Research: Atmospheres*, *124*(22), 12282–12300. https://doi.org/10.1029/2019JD030792

Bozlaker, A., Spada, N. J., Fraser, M. P., & Chellam, S. (2014). Elemental characterization of $PM_{2.5}$ and PM_{10} emitted from light duty vehicles in the Washburn Tunnel of Houston, Texas: Release of rhodium, palladium, and platinum. *Environmental Science and Technology*, *48*(1), 54–62. https://doi.org/10.1021/es4031003

Brahney, J., Mahowald, N., Ward, D. S., Ballantyne, A. P., & Neff, J. C. (2015). Is atmospheric phosphorus pollution altering global alpine Lake stoichiometry? *Global Biogeochemical Cycles*, *29*(9), 1369–1383. https://doi.org/10.1002/2015GB005137

Carling, G. T., Rupper, S. B., Fernandez, D. P., Tingey, D. G., & Harrison, C. B. (2017). Effect of atmospheric deposition and weathering on trace element concentrations in glacial meltwater at Grand Teton National Park, Wyoming, U.S.A. *Arctic, Antarctic, and Alpine Research*, *49*(3), 427–440. https://doi.org/10.1657/AAAR0016.071

Charter, R. A., Tabatabai, M. A., & Schafer, J. W. (1995). Arsenic, molybdenum, selenium, and tungsten contents of distinct fertilizers and phosphate rocks. *Communications in Soil Science and Plant Analysis*, *26*(17–18), 3051–3062. https://doi.org/10.1080/00103629509369508

Computational and Information Systems Laboratory (2019). *Cheyenne: HPE/SGI ICE XA System (NCAR Community Computing)*. Boulder, CO: National Center for Atmospheric Research. Retrieved from https://doi.org/10.5065/D6RX99HX

Dai, A., & Trenberth, K. E. (2002). Estimates of freshwater discharge from continents: Latitudinal and seasonal variations. *Journal of Hydrometeorology*, *3*(6), 660–687. https://doi.org/10.1175/1525-7541(2002)003<0660:EOFDFC>2.0.CO;2

Danadurai, K. S. K., Chellam, S., Lee, C.-T., & Fraser, M. P. (2011). Trace elemental analysis of airborne particulate matter using dynamic reaction cell inductively coupled plasma – mass spectrometry: Application to monitoring episodic industrial emission events. *Analytica Chimica Acta*, *686*(1–2), 40–49. https://doi.org/10.1016/j.aca.2010.11.037

Darnajoux, R., Magain, N., Renaudin, M., Lutzoni, F., Bellenger, J., & Zhang, X. (2019). Molybdenum threshold for ecosystem scale alternative vanadium nitrogenase activity in boreal forests. *Proceedings of the National Academy of Sciences*, *116*(49), 24682–24688. https://doi.org/10.1073/pnas.1913314116

Darnajoux, R., Zhang, X., McRose, D. L., Miadlikowska, J., Lutzoni, F., Kraepiel, A. M. L., & Bellenger, J. P. (2017). Biological nitrogen fixation by alternative nitrogenases in boreal cyanolichens: importance of molybdenum availability and implications for current biological nitrogen fixation estimates. *New Phytologist*, *213*(2), 680–689. https://doi.org/10.1111/nph.14166

Das, S., & Chellam, S. (2020). Estimating light-duty vehicles' contributions to ambient $PM_{2.5}$ and PM_{10} at a near-highway urban elementary school via elemental characterization emphasizing rhodium, palladium, and platinum. *Science of The Total Environment*, *747*, 141268. https://doi.org/10.1016/j.scitotenv.2020.141268

da Silva, L. I. D., de Souza Sarkis, J. E., Zotin, F. M. Z., Carneiro, M. C., Neto, A. A., da Silvados, A. S. A. G., et al. (2008). Traffic and catalytic converter – Related atmospheric contamination in the metropolitan region of the city of Rio de Janeiro, Brazil. *Chemosphere*, *71*(4), 677–684. https://doi.org/10.1016/j.chemosphere.2007.10.057

Davidson, E. A., de Carvalho, C. J. R., Figueira, A. M., Ishida, F. Y., Ometto, J. P. H. B., Nardoto, G. B., et al. (2007). Recuperation of nitrogen cycling in Amazonian forests following agricultural abandonment. *Nature*, *447*(7147), 995–998. https://doi.org/10.1038/nature05900

DEFRA (2020). *UK Air Information Resource Monitoring Data*, London, UK: Department for Environment, Food and Rural Affairs. Retrieved from https://uk-air.defra.gov.uk/data/

De Mello, L. F., Baldanza, M. A. S., Noronha, F. B., & Schmal, M. (2003). NO reduction with ethanol on MoO_3/Al_2O_3 and CeO_2-ZrO_2-supported Pd catalysts. *Catalysis Today*, *85*(1), 3–12. https://doi.org/10.1016/S0920-5861(03)00188-3

Dentener, F., Drevet, J., Lamarque, J. F., Bey, I., Eickhout, B., Fiore, A. M., et al. (2006). Nitrogen and sulfur deposition on regional and global scales: A multimodel evaluation. *Global Biogeochemical Cycles*, *20*(4), 1–21. https://doi.org/10.1029/2005GB002672

Derimian, Y., Karnieli, A., Kaufman, Y. J., Andreae, M. O., Andreae, T. W., Dubovik, O., et al. (2006). Dust and pollution aerosols over the Negev desert, Israel: Properties, transport and radiative forcing. *Journal of Geophysical Research*, *111*(D5), D05205, 1–14. https://doi.org/10.1029/2005JD006549

Desboeufs, K. V., Sofikitis, A., Losno, R., Colin, J. L., & Ausset, P. (2005). Dissolution and solubility of trace metals from natural and anthropogenic aerosol particulate matter. *Chemosphere*, *58*(2), 195–203. https://doi.org/10.1016/j.chemosphere.2004.02.025

DFM and WSP (2020). *Diagnóstico de Riesgo Ambiental, Región de Antofagasta. Componente A) Estudio de calidad del aire por presencia de material particulado sedimentable en la ciudad de Antofagasta*, Ministerio del Medio Ambiente. Antofagasta, Chile. Retrieved from https://mma.gob.cl/antofagasta/

Dillner, A. M., Schauer, J. J., Christensen, W. F., & Cass, G. R. (2005). A quantitative method for clustering size distributions of elements. *Atmospheric Environment*, *39*(8), 1525–1537. https://doi.org/10.1016/j.atmosenv.2004.11.035

Dongarrà, G., Manno, E., Varrica, D., Lombardo, M., & Vultaggio, M. (2010). Study on ambient concentrations of PM_{10}, $PM_{10-2.5}$, $PM_{2.5}$ and gaseous pollutants. Trace elements and chemical speciation of atmospheric particulates. *Atmospheric Environment*, *44*(39), 5244–5257. https://doi.org/10.1016/j.atmosenv.2010.08.041

Dongarrà, G., Manno, E., Varrica, D., & Vultaggio, M. (2007). Mass levels, crustal component and trace elements in PM_{10} in Palermo, Italy. *Atmospheric Environment*, *41*(36), 7977–7986. https://doi.org/10.1016/j.atmosenv.2007.09.015

Dynarski, K. A., & Houlton, B. Z. (2018). Nutrient limitation of terrestrial free-living nitrogen fixation. *New Phytologist*, *217*(3), 1050–1061. https://doi.org/10.1111/nph.14905

Eady, R. R. (1996). Structure−function relationships of alternative nitrogenases. *Chemical Reviews*, *96*(7), 3013–3030. https://doi.org/10.1021/cr950057h

European Monitoring and Evaluation Programme (2020). *European Monitoring and Evaluation Programme*, *Convention on Long-range Transboundary Air Pollution (LRTAP)*. Retrieved from https://www.emep.int/

Fujiwara, F., Rebagliati, R. J., Dawidowski, L., Gómez, D., Polla, G., Pereyra, V., & Smichowski, P. (2011). Spatial and chemical patterns of size fractionated road dust collected in a megacitiy. *Atmospheric Environment*, *45*(8), 1497–1505. https://doi.org/10.1016/j.atmosenv.2010.12.053

Fuzzi, S., Decesari, S., Facchini, M. C., Cavalli, F., Emblico, L., Mircea, M., et al. (2007). Overview of the inorganic and organic composition of size-segregated aerosol in Rondônia, Brazil, from the biomass-burning period to the onset of the wet season. *Journal of Geophysical Research*, *112*(D1), D01201. https://doi.org/10.1029/2005JD006741

Ge, S., Bai, Z., Liu, W., Zhu, T., Wang, T., Qing, S., & Zhang, J. (2001). Boiler briquette coal versus raw coal: Part I—Stack gas emissions. *Journal of the Air and Waste Management Association*, *51*(4), 524–533. https://doi.org/10.1080/10473289.2001.10464293

Gelaro, R., McCarty, W., Suárez, M. J., Todling, R., Molod, A., Takacs, L., et al. (2017). The Modern-Era Retrospective Analysis for Research and Applications, Version 2 (MERRA-2). *Journal of Climate*, *30*(14), 5419–5454 https://doi.org/10.1175/JCLI-D-16-0758.1

Gianini, M. F. D., Fischer, A., Gehrig, R., Ulrich, A., Wichser, A., Piot, C., et al. (2012a). Comparative source apportionment of PM_{10} in Switzerland for 2008/2009 and 1998/1999 by Positive Matrix Factorisation. *Atmospheric Environment*, *54*, 149–158. https://doi.org/10.1016/j.atmosenv.2012.02.036

Gianini, M. F. D., Gehrig, R., Fischer, A., Ulrich, A., Wichser, A., & Hueglin, C. (2012b). Chemical composition of PM_{10} in Switzerland: An analysis for 2008/2009 and changes since 1998/1999. *Atmospheric Environment*, *54*, 97–106. https://doi.org/10.1016/j.atmosenv.2012.02.037

Ginoux, P., Prospero, J. M., Gill, T. E., Hsu, N. C., & Zhao, M. (2012). Global-scale attribution of anthropogenic and natural dust sources and their emission rates based on MODIS Deep Blue aerosol products. *Reviews of Geophysics*, *50*(3), 1–36. https://doi.org/10.1029/2012RG000388

Glass, J. B., Axler, R. P., Chandra, S., & Goldman, C. R. (2012). Molybdenum limitation of microbial nitrogen assimilation in aquatic ecosystems and pure cultures. *Frontiers in Microbiology*, *3*(September), 1–11. https://doi.org/10.3389/fmicb.2012.00331

Gonet, T., & Maher, B. A. (2019). Airborne, vehicle-derived Fe-bearing nanoparticles in the urban environment: A review. *Environmental Science and Technology*, *53*(17), 9970–9991. https://doi.org/10.1021/acs.est.9b01505

Graham, B., Guyon, P., Maenhaut, W., Taylor, P. E., Ebert, M., Matthias-Maser, S., et al. (2003). Composition and diurnal variability of the natural Amazonian aerosol. *Journal of Geophysical Research*, *108*(D24), 4765. https://doi.org/10.1029/2003JD004049

Grigoratos, T., & Martini, G. (2014). *Non-exhaust traffic related emissions. Brake and tyre wear PM*. JRC Science and Policy Reports Luxembourg: European Union. Retrieved from https://doi.org/10.2790/21481

Grigoratos, T., & Martini, G. (2015). Brake wear particle emissions: A review. *Environmental Science and Pollution Research*, *22*(4), 2491–2504. https://doi.org/10.1007/s11356-014-3696-8

Hand, J. L., Gill, T. E., & Schichtel, B. A. (2017). Spatial and seasonal variability in fine mineral dust and coarse aerosol mass at remote sites across the United States. *Journal of Geophysical Research: Atmospheres*, *122*(5), 3080–3097. https://doi.org/10.1002/2016JD026290

Hand, J. L., Gill, T. E., & Schichtel, B. A. (2019). Urban and rural coarse aerosol mass across the United States: Spatial and seasonal variability and long-term trends. *Atmospheric Environment*, *218*(September), 117025. https://doi.org/10.1016/j.atmosenv.2019.117025

Hansen, M. C., Potapov, P. V., Moore, R., Hancher, M., Turubanova, S. A., Tyukavina, A., et al. (2013). High-resolution global maps of 21st-century forest cover change. *Science*, *342*(November), 850–854. https://doi.org/10.1126/science.1244693

Harrison, R. M., Jones, A. M., Gietl, J., Yin, J., & Green, D. C. (2012). Estimation of the contributions of brake dust, tire wear, and resuspension to nonexhaust traffic particles derived from atmospheric measurements. *Environmental Science and Technology*, *46*(12), 6523–6529. https://doi.org/10.1021/es300894r

Heimburger, A., Losno, R., Triquet, S., Dulac, F., & Mahowald, N. (2012). Direct measurement of atmospheric iron, cobalt and aluminum-derived dust deposition at Kerguelen Islands. *Global Biogeochemical Cycles*, *26*(4), GB4016, 1–14. https://doi.org/10.1029/2012GB004301

Hernández-Pellón, A., & Fernández-Olmo, I. (2019). Airborne concentration and deposition of trace metals and metalloids in an urban area downwind of a manganese alloy plant. *Atmospheric Pollution Research*, *10*(3), 712–721. https://doi.org/10.1016/j.apr.2018.11.009

Houlton, B. Z., Wang, Y.-P., Vitousek, P. M., & Field, C. B. (2008). A unifying framework for dinitrogen fixation in the terrestrial biosphere. *Nature*, *454*(7202), 327–330. https://doi.org/10.1038/nature07028

Hsu, C. Y., Chiang, H. C., Lin, S. L., Chen, M. J., Lin, T. Y., & Chen, Y. C. (2016). Elemental characterization and source apportionment of PM_{10} and $PM_{2.5}$ in the western coastal area of central Taiwan. *Science of the Total Environment*, *541*, 1139–1150. https://doi.org/10.1016/j.scitotenv.2015.09.122

Hsu, S.-C., Wong, G. T. F., Gong, G.-C., Shiah, F.-K., Huang, Y.-T., Kao, S.-J., et al. (2010). Sources, solubility, and dry deposition of aerosol trace elements over the East China Sea. *Marine Chemistry*, *120*(1–4), 116–127. https://doi.org/10.1016/j.marchem.2008.10.003

Hueglin, C., Gehrig, R., Baltensperger, U., Gysel, M., Monn, C., & Vonmont, H. (2005). Chemical characterisation of $PM_{2.5}$, PM_{10} and coarse particles at urban, near-city and rural sites in Switzerland. *Atmospheric Environment*, *39*(4), 637–651. https://doi.org/10.1016/j.atmosenv.2004.10.027

Hulskotte, J. H. J., Roskam, G. D., & Denier van der Gon, H. A. C. (2014). Elemental composition of current automotive braking materials and derived air emission factors. *Atmospheric Environment*, *99*, 436–445. https://doi.org/10.1016/j.atmosenv.2014.10.007

Hungate, B. A., Stiling, P. D., Dijkstra, P., Johnson, D. W., Ketterer, M. E., Hymus, G. J., et al. (2004). CO_2 elicits long-term decline in nitrogen fixation. *Science*, *304*(5675), 1291. https://doi.org/10.1126/science.1095549

Hurrell, J. W., Holland, M. M., Gent, P. R., Ghan, S., Kay, J. E., Kushner, P. J., et al. (2013). The community earth system model: A framework for collaborative research. *Bulletin of the American Meteorological Society*, *94*(9), 1339–1360. https://doi.org/10.1175/BAMS-D-12-00121.1

Hurtt, G. C., Chini, L. P., Frolking, S., Betts, R. A., Feddema, J., Fischer, G., et al. (2011). Harmonization of land-use scenarios for the period 1500-2100: 600 years of global gridded annual land-use transitions, wood harvest, and resulting secondary lands. *Climatic Change*, *109*(1–2), 117–161. https://doi.org/10.1007/s10584-011-0153–2

Izquierdo, M., & Querol, X. (2012). Leaching behaviour of elements from coal combustion fly ash: An overview. *International Journal of Coal Geology*, *94*, 54–66. https://doi.org/10.1016/j.coal.2011.10.006

Jang, H. N., Seo, Y. C., Lee, J. H., Hwang, K. W., Yoo, J. I., Sok, C. H., & Kim, S. H. (2007). Formation of fine particles enriched by V and Ni from heavy oil combustion: Anthropogenic sources and drop-tube furnace experiments. *Atmospheric Environment*, *41*(5), 1053–1063. https://doi.org/10.1016/j.atmosenv.2006.09.011

Kauffman, J. B., Cummings, D. L., Ward, D. E., & Babbitt, R. (1995). Fire in the Brazilian Amazon: 1. Biomass, nutrient pools, and losses in slashed primary forests. *Oecologia*, *104*(4), 397–408. https://doi.org/10.1007/BF00341336

Kok, J. F., Mahowald, N. M., Fratini, G., Gillies, J. A., Ishizuka, M., Leys, J. F., et al. (2014a). An improved dust emission model – Part 1: Model description and comparison against measurements. *Atmospheric Chemistry and Physics*, *14*(23), 13023–13041 https://doi.org/10.5194/acp-14-13023-2014

Kok, J. F., Albani, S., Mahowald, N. M., & Ward, D. S. (2014b). An improved dust emission model – Part 2: Evaluation in the Community Earth System Model, with implications for the use of dust source functions. *Atmospheric Chemistry and Physics*, *14*(23), 13043–13061. https://doi.org/10.5194/acp-14-13043-2014

Kok, J. F., Ridley, D. A., Zhou, Q., Miller, R. L., Zhao, C., Heald, C. L., et al. (2017). Smaller desert dust cooling effect estimated from analysis of dust size and abundance. *Nature Geoscience*, *10*(4), 274–278. https://doi.org/10.1038/ngeo2912

Laing, J. R., Hopke, P. K., Hopke, E. F., Husain, L., Dutkiewicz, V. A., Paatero, J., & Viisanen, Y. (2013). Long-term trends of biogenic sulfur aerosol and its relationship with sea surface temperature in Arctic Finland. *Journal of Geophysical Research: Atmospheres*, *118*(20), 11770–11776. https://doi.org/10.1002/2013JD020384

Laing, J. R., Hopke, P. K., Hopke, E. F., Husain, L., Dutkiewicz, V. A., Paatero, J., & Viisanen, Y. (2014a). Long-term particle measurements in Finnish Arctic: Part I – Chemical composition and trace metal solubility. *Atmospheric Environment*, *88*, 275–284. https://doi.org/10.1016/j.atmosenv.2014.03.002

Laing, J. R., Hopke, P. K., Hopke, E. F., Husain, L., Dutkiewicz, V. A., Paatero, J., & Viisanen, Y. (2014b). Long-term particle measurements in Finnish Arctic: Part II – Trend analysis and source location identification. *Atmospheric Environment*, *88*, 285–296. https://doi.org/10.1016/j.atmosenv.2014.01.015

LeBauer, D. S., & Treseder, K. K. (2008). Nitrogen limitation of net primary productivity in terrestrial ecosystems is globally distributed. *Ecology*, *89*(2), 371–379. https://doi.org/10.1890/06-2057.1

Li, L., Mahowald, N., Miller, R. L., Perez Garcia-Pando, C., Klose, M., Hamilton, D. S., et al. (2020). Quantifying the range of the dust direct radiative effect due to source mineralogy uncertainty. *Atmospheric Chemistry and Physics Discussions.* https://doi.org/10.5194/acp-2020-547

Liu, X., Easter, R. C., Ghan, S. J., Zaveri, R., Rasch, P., Shi, X., et al. (2011). Toward a minimal representation of aerosol direct and indirect effects: Model description and evaluation. *Geoscientific Model Development Discussions*, *4*(4), 3485–3598. https://doi.org/10.5194/gmdd-4-3485-2011

Machado, J. G. M. da S., Brehm, F. A., Moraes, C. A. M., dos Santos, C. A., & Vilela, A. C. F. (2006). Characterization study of electric arc furnace dust phases. *Materials Research*, *9*(1), 41–45. https://doi.org/10.1590/s1516-14392006000100009

Machemer, S. D. (2004). Characterization of airborne and bulk particulate from iron and steel manufacturing facilities. *Environmental Science & Technology*, *38*(2), 381–389. https://doi.org/10.1021/es020897v

Maenhaut, W., & Cafmeyer, J. (1998). Long-term atmospheric aerosol study at urban and rural sites in Belgium using multi-elemental analysis by particle-induced X-Ray emission spectrometry and short-irradiation instrumental neutron activation analysis. *X-Ray Spectrometry*, *27*(4), 236–246. https://doi.org/10.1002/(SICI)1097-4539(199807/08)27:4<236::AID-XRS292>3.0.CO;2-F

Maenhaut, W., Cafmeyer, J., Ptasinski, J., Andreae, M. O., Andreae, T. W., Elbert, W., et al. (1997a). Chemical composition and light scattering of the atmospheric aerosol at a remote site in the Negev Desert, Israel. *Journal of Aerosol Science*, *28*(Supplement 1), S73–S74. https://doi.org/10.1016/S0021-8502(97)85037-9

Maenhaut, W., De Ridder, D. J. A., Fernandez-Jimenez, M.-T., Hooper, M. A., Hooper, B., & Nurhayati, M. (2002a). Long-term observations of regional aerosol composition at two sites in Indonesia. *Nuclear Instruments and Methods in Physics Research Section B: Beam Interactions with Materials and Atoms*, *189*(1–4), 259–265. https://doi.org/10.1016/S0168-583X(01)01054-0

Maenhaut, W., Fernández-Jiménez, M.-T., & Artaxo, P. (1999). Long-term study of atmospheric aerosols in Cuiaba, Brazil: Multielemental composition, sources and source apportionment. *Journal of Aerosol Science*, *30*(Supplement 1), S259–S260.

Maenhaut, W., Fernández-Jiménez, M.-T., Rajta, I., & Artaxo, P. (2002b). Two-year study of atmospheric aerosols in Alta Floresta, Brazil: Multielemental composition and source apportionment. *Nuclear Instruments and Methods in Physics Research Section B: Beam Interactions with Materials and Atoms*, *189*(1–4), 243–248. https://doi.org/10.1016/S0168-583X(01)01050-3

Maenhaut, W., Fernández-Jiménez, M.-T., Rajta, I., Dubtsov, S., Meixner, F. X., Andreae, M. O., et al. (2000a). Long-term aerosol composition measurements and source apportionment at Rukomechi, Zimbabwe. *Journal of Aerosol Science*, *31*(Supplement 1), 228–229. https://doi.org/10.1016/S0021-8502(00)90237-4

Maenhaut, W., Fernández-Jiménez, M.-T., Vanderzalm, J. L., Hooper, B., Hooper, M. A., & Tapper, N. J. (2000b). Aerosol composition at Jabiru, Australia, and impact of biomass burning. *Journal of Aerosol Science*, *31*(Supplement 1), 745–746 https://doi.org/10.1016/S0021-8502(00)90755-9

Maenhaut, W., Francois, F., Cafmeyer, J., Gilot, C., & Hanssen, J. E. (1997b). Long-term aerosol study in southern Norway, and the relationship of aerosol components to source regions. In P. M. Borrell (Ed.), *Proceedings of Eurotrac Symposium '96: Transport and transformation of pollutants in the troposphere*. Clouds, aerosols, modelling and photo-oxidants (*1*, pp. 277–280). South Hampton, UK: Computational Mechanics.

Maenhaut, W., Koppen, G., & Artaxo, P. (1996a). Long-term atmospheric aerosol study in Cuiaba, Brazil: Multielemental composition, sources, and impact of biomass burning. In J. S. Levine (Ed.), Biomass burning and global change: Biomass Burning in South America, Southeast Asia, and Temperate and Boreal Ecosystems, and the Oil Fires of Kuwait (2, pp. 637–652). Cambridge Massachusetts: MIT Press.

Maenhaut, W., Nava, S., Lucarelli, F., Wang, W., Chi, X., & Kulmala, M. (2011). Chemical composition, impact from biomass burning, and mass closure for $PM_{2.5}$ and PM_{10} aerosols at Hyytiälä, Finland, in summer 2007. *X-Ray Spectrometry*, *40*(3), 168–171. https://doi.org/10.1002/xrs.1302

Maenhaut, W., Raes, N., Chi, X., Cafmeyer, J., & Wang, W. (2008). Chemical composition and mass closure for $PM_{2.5}$ and PM_{10} aerosols at K-puszta, Hungary, in summer 2006. *X-Ray Spectrometry*, *37*(2), 193–197. https://doi.org/10.1002/xrs.1062

Maenhaut, W., Raes, N., Chi, X., Cafmeyer, J., Wang, W., & Salma, I. (2005). Chemical composition and mass closure for fine and coarse aerosols at a kerbside in Budapest, Hungary, in spring 2002. *X-Ray Spectrometry*, *34*(4), 290–296. https://doi.org/10.1002/xrs.820

Maenhaut, W., Salma, I., Cafmeyer, J., Annegarn, H. J., & Andreae, M. O. (1996b). Regional atmospheric aerosol composition and sources in the eastern Transvaal, South Africa, and impact of biomass burning. *Journal of Geophysical Research*, *101*(19), 23631–23650. https://doi.org/10.1029/95jd02930

Maenhaut, W., Salomonovic, R., Cafmeyer, J., Ichoku, C., Karnieli, A., & Andreae, M. O. (1996c). Anthropogenic and natural radiatively active aerosol types at Sede Boker, Israel. *Journal of Aerosol Science*, *27*(Supplement 1), 47–48. https://doi.org/10.1016/0021-8502(96)00096-1

Mahowald, N., Albani, S., Kok, J. F., Engelstaeder, S., Scanza, R., Ward, D. S., & Flanner, M. G. (2014). The size distribution of desert dust aerosols and its impact on the Earth system. *Aeolian Research*, *15*, 53–71. https://doi.org/10.1016/j.aeolia.2013.09.002

Mahowald, N., Jickells, T. D., Baker, A. R., Artaxo, P., Benitez-Nelson, C. R., Bergametti, G., et al. (2008). Global distribution of atmospheric phosphorus sources, concentrations and deposition rates, and anthropogenic impacts. *Global Biogeochemical Cycles*, *22*(4), 1–19. https://doi.org/10.1029/2008GB003240

Mahowald, N., Ward, D. S., Kloster, S., Flanner, M. G., Heald, C. L., Heavens, N. G., et al. (2011). Aerosol impacts on climate and biogeochemistry. *Annual Review of Environment and Resources*, *36*, 45–74. https://doi.org/10.1146/annurev-environ-042009-094507

Mahowald, N. M., Artaxo, P., Baker, A. R., Jickells, T. D., Okin, G. S., Randerson, J. T., & Townsend, A. R. (2005). Impacts of biomass burning emissions and land use change on Amazonian atmospheric phosphorus cycling and deposition. *Global Biogeochemical Cycles*, *19*(4), 1–15. https://doi.org/10.1029/2005GB002541

Martin, J., & Meybeck, M. (1979). Elemental mass-balance of material carried by major world rivers. *Marine Chemistry*, *7*(3), 173–206.

McRose, D. L., Zhang, X., Kraepiel, A. M. L., & Morel, F. M. M. (2017). Diversity and activity of alternative nitrogenases in sequenced genomes and coastal environments. *Frontiers in Microbiology*, *8*(February), 1–13. https://doi.org/10.3389/fmicb.2017.00267

Meij, R. (1994). Trace element behavior in coal-fired power plants. *Fuel Processing Technology*, *39*(1–3), 199–217.

Meskhidze, N., Chameides, W. L., & Nenes, A. (2005). Dust and pollution: A recipe for enhanced ocean fertilization? *Journal of Geophysical Research*, *110*(3), 1–23. https://doi.org/10.1029/2004JD005082

Mkoma, S. L., Maenhaut, W., Chi, X., Wang, W., & Raes, N. (2009a). Characterisation of PM_{10} atmospheric aerosols for the wet season 2005 at two sites in East Africa. *Atmospheric Environment*, *43*(3), 631–639. https://doi.org/10.1016/j.atmosenv.2008.10.008

Mkoma, S. L., Maenhaut, W., Chi, X., Wang, W., & Raes, N. (2009b). Chemical composition and mass closure for PM_{10} aerosols during the 2005 dry season at a rural site in Morogoro, Tanzania. *X-Ray Spectrometry*, *38*(4), 293–300. https://doi.org/10.1002/xrs.1179

Mkoma, S. L., Wang, W., & Maenhaut, W. (2009c). Seasonal variation of water-soluble inorganic species in the coarse and fine atmospheric aerosols at Dar es Salaam, Tanzania. *Nuclear Instruments and Methods in Physics Research Section B: Beam Interactions with Materials and Atoms*, *267*(17), 2897–2902. https://doi.org/10.1016/j.nimb.2009.06.099

Moreno, N., Querol, X., Andres, J. M., Stanton, K., Towler, M., Nugteren, H., et al. (2005). Physico-chemical characteristics of European pulverized coal combustion fly ashes. *Fuel*, *84*(11), 1351–1363. https://doi.org/10.1016/j.fuel.2004.06.038

Morera-Gómez, Y., Alonso-Hernández, C. M., Santamaría, J. M., Elustondo, D., Lasheras, E., & Widory, D. (2020). Levels, spatial distribution, risk assessment, and sources of environmental contamination vectored by road dust in Cienfuegos (Cuba) revealed by chemical and C and N stable isotope compositions. *Environmental Science and Pollution Research*, *27*(2), 2184–2196. https://doi.org/10.1007/s11356-019-06783-7

Morera-Gómez, Y., Elustondo, D., Lasheras, E., Alonso-Hernández, C. M., & Santamaría, J. M. (2018). Chemical characterization of PM_{10} samples collected simultaneously at a rural and an urban site in the Caribbean coast: Local and long-range source apportionment. *Atmospheric Environment*, *192*(August), 182–192. https://doi.org/10.1016/j.atmosenv.2018.08.058

NPCS Board of Consultants & Engineers (2009). *Handbook on rare Earth metals and alloys (properties, extraction, preparation and applications)*, Delhi, India: Asia Pacific Business Press, Inc.

Nriagu, J. O. (1989). A global assessment of natural sources of atmospheric trace metals. *Nature*, *338*(6210), 47–49. https://doi.org/10.1038/338047a0

Nriagu, J. O., & Pacyna, J. M. (1988). Quantitative assessment of worldwide contamination of air, water and soils by trace metals. *Nature*, *333*(6169), 134–139. https://doi.org/10.1038/333134a0

Nyanganyura, D., Maenhaut, W., Mathuthu, M., Makarau, A., & Meixner, F. X. (2007). The chemical composition of tropospheric aerosols and their contributing sources to a continental background site in northern Zimbabwe from 1994 to 2000. *Atmospheric Environment*, *41*(12), 2644–2659. https://doi.org/10.1016/j.atmosenv.2006.11.015

O'Dowd, C. D., & de Leeuw, G. (2007). Marine aerosol production: A review of the current knowledge. *Philosophical Transactions of the Royal Society A: Mathematical, Physical and Engineering Sciences*, *365*(1856), 1753–1774. https://doi.org/10.1098/rsta.2007.2043

Okin, G. S., Mahowald, N., Chadwick, O. A., & Artaxo, P. (2004). Impact of desert dust on the biogeochemistry of phosphorus in terrestrial ecosystems. *Global Biogeochemical Cycles*, *18*(2). https://doi.org/10.1029/2003GB002145

Peñuelas, J., Poulter, B., Sardans, J., Ciais, P., Van Der Velde, M., Bopp, L., et al. (2013). Human-induced nitrogen-phosphorus imbalances alter natural and managed ecosystems across the globe. *Nature Communications*, *4*, 2934, 1–10. https://doi.org/10.1038/ncomms3934

Peñuelas, J., Sardans, J., Rivas-ubach, A., & Janssens, I. A. (2012). The human-induced imbalance between C, N and P in Earth's life system. *Global Change Biology*, *18*(1), 3–6. https://doi.org/10.1111/j.1365-2486.2011.02568.x

Perakis, S. S., Pett-Ridge, J. C., & Catricala, C. E. (2017). Nutrient feedbacks to soil heterotrophic nitrogen fixation in forests. *Biogeochemistry*, *134*(1), 41–55. https://doi.org/10.1007/s10533-017-0341-x

Pérez, N., Pey, J., Querol, X., Alastuey, A., López, J. M., & Viana, M. (2008). Partitioning of major and trace components in PM_{10}-$PM_{2.5}$-PM_1 at an urban site in Southern Europe. *Atmospheric Environment*, *42*(8), 1677–1691. https://doi.org/10.1016/j.atmosenv.2007.11.034

Prospero, J. M., Barrett, K., Church, T., Dentener, F., Duce, R. A., Galloway, J. N., et al. (1996). Atmospheric deposition of nutrients to the North Atlantic Basin. *Biogeochemistry*, *35*(1), 27–73. https://doi.org/10.1007/BF02179824

Putaud, J.-P., Raes, F., Van Dingenen, R., Brüggemann, E., Facchini, M.-C., Decesari, S., et al. (2004). A European aerosol phenomenology—2: Chemical characteristics of particulate matter at kerbside, urban, rural and background sites in Europe. *Atmospheric Environment*, *38*(16), 2579–2595. https://doi.org/10.1016/j.atmosenv.2004.01.041

Putaud, J.-P., Van Dingenen, R., Alastuey, A., Bauer, H., Birmili, W., Cyrys, J., et al. (2010). A European aerosol phenomenology – 3: Physical and chemical characteristics of particulate matter from 60 rural, urban, and kerbside sites across Europe. *Atmospheric Environment*, *44*(10), 1308–1320. https://doi.org/10.1016/j.atmosenv.2009.12.011

Qu, Z., Trabelsi, A., Losno, R., Monna, F., Nowak, S., Masmoudi, M., & Quisefit, J. P. (2020). A laboratory dust generator applying vibration to soil sample: mineralogical study and compositional analyses. *Journal of Geophysical Research: Atmospheres*, *125*(7), 1–10. https://doi.org/10.1029/2019JD032224

Querol, X., Fernández-Turiel, J., & López-Soler, A. (1995). Trace elements in coal and their behaviour during combustion in a large power station. *Fuel*, *74*(3), 331–343. https://doi.org/10.1016/0016-2361(95)93464-O

R Core Team (2018). *R: A language and environment for statistical computing*. Vienna, Austria: R Foundation for Statistical Computing.

Rathod, S. D., Hamilton, D. S., Mahowald, N. M., Klimont, Z., Corbett, J. J., & Bond, T. C. (2020). A mineralogy-based anthropogenic combustion-iron emission inventory. *Journal of Geophysical Research: Atmospheres*, *125*(17), 1–35. https://doi.org/10.1029/2019JD032114

Rauch, J. N., & Pacyna, J. M. (2009). Earth's global Ag, Al, Cr, Cu, Fe, Ni, Pb, and Zn cycles. *Global Biogeochemical Cycles*, *23*(2), 1–16. https://doi.org/10.1029/2008GB003376

Reed, S. C., Cleveland, C. C., & Townsend, A. R. (2013). Relationships among phosphorus, molybdenum and free-living nitrogen fixation in tropical rain forests: Results from observational and experimental analyses. *Biogeochemistry*, *114*(1–3), 135–147. https://doi.org/10.1007/s10533-013-9835-3

Ridley, D. A., Heald, C. L., Kok, J. F., & Zhao, C. (2016). An observationally constrained estimate of global dust aerosol optical depth. *Atmospheric Chemistry and Physics*, *16*(23), 15097–15117. https://doi.org/10.5194/acp-16-15097-2016

Robertson, J. M., Nesbitt, J. A., & Lindsay, M. B. J. (2019). Aqueous- and solid-phase molybdenum geochemistry of oil sands fluid petroleum coke deposits, Alberta, Canada. *Chemosphere*, *217*, 715–723. https://doi.org/10.1016/j.chemosphere.2018.11.064

Rodríguez, S., Alastuey, A., Alonso-Pérez, S., Querol, X., Cuevas, E., Abreu-Afonso, J., et al. (2011). Transport of desert dust mixed with North African industrial pollutants in the subtropical Saharan Air Layer. *Atmospheric Chemistry and Physics*, *11*(13), 6663–6685. https://doi.org/10.5194/acp-11-6663-2011

Rodríguez, S., Cuevas, E., Prospero, J. M., Alastuey, A., Querol, X., López-Solano, J., et al. (2015). Modulation of Saharan dust export by the North African dipole. *Atmospheric Chemistry and Physics*, *15*(13), 7471–7486. https://doi.org/10.5194/acp-15-7471-2015

Romero, I. C., Klein, N. J., Sañudo-Wilhelmy, S. A., & Capone, D. G. (2013). Potential trace metal co-limitation controls on N_2 fixation and NO_3^- uptake in lakes with varying trophic status. *Frontiers in Microbiology*, *4*, 54. https://doi.org/10.3389/fmicb.2013.00054

Rousk, K., Degboe, J., Michelsen, A., Bradley, R., & Bellenger, J. (2016). Molybdenum and phosphorus limitation of moss-associated nitrogen fixation in boreal ecosystems. *New Phytologist*, *214*(1), 97–107. https://doi.org/10.1111/nph.14331

Rudnick, R. L., & Gao, S. (2003). Composition of the continental crust. In R. L. Rudnick (Ed.), *The crust* (pp. 1–64). Amsterdam: Elsevier.

Ryder, C. L., Highwood, E. J., Walser, A., Seibert, P., Philipp, A., & Weinzierl, B. (2019). Coarse and giant particles are ubiquitous in Saharan dust export regions and are radiatively significant over the Sahara. *Atmospheric Chemistry and Physics Discussions*, *19*(24), 15353–15376. https://doi.org/10.5194/acp-2019-421

Salma, I., Maenhaut, W., Annegarn, H. J., Andreae, M. O., Meixner, F. X., & Garstang, M. (1997). Combined application of INAA and PIXE for studying the regional aerosol composition in southern Africa. *Journal of Geophsyical Research*, *216*(1), 143–148. https://doi.org/10.1007/BF02034512

Scanza, R. A., Mahowald, N., Ghan, S., Zender, C. S., Kok, J. F., Liu, X., et al. (2015). Modeling dust as component minerals in the Community Atmosphere Model: Development of framework and impact on radiative forcing. *Atmospheric Chemistry and Physics*, *15*(1), 537–561. https://doi.org/10.5194/acp-15-537-2015

Schlesinger, W. H., Klein, E. M., & Vengosh, A. (2017). Global biogeochemical cycle of vanadium. *Proceedings of the National Academy of Sciences*, *114*(52), E11092–E11100. https://doi.org/10.1073/pnas.1715500114

Schmal, M., Baldanza, M. A. S., & Vannice, M. A. (1999). Pd-xMo/Al$_2$O$_3$ catalysts for NO reduction by CO. *Journal of Catalysis*, *185*(1), 138–151. https://doi.org/10.1006/jcat.1999.2465

Schutgens, N. A. J., Gryspeerdt, E., Weigum, N., Tsyro, S., Goto, D., Schulz, M., & Stier, P. (2016). Will a perfect model agree with perfect observations? The impact of spatial sampling. *Atmospheric Chemistry and Physics*, *16*(10), 6335–6353. https://doi.org/10.5194/acp-16-6335-2016

Sedwick, P. N., Sholkovitz, E. R., & Church, T. M. (2007). Impact of anthropogenic combustion emissions on the fractional solubility of aerosol iron: Evidence from the Sargasso Sea. *Geochemistry, Geophysics, Geosystems*, *8*(10), 1–21. https://doi.org/10.1029/2007GC001586

Selin, N. E. (2009). Global biogeochemical cycling of mercury: A review. *Annual Review of Environment and Resources*, *34*(1), 43–63. https://doi.org/10.1146/annurev.environ.051308.084314

Sen, I. S., & Peucker-Ehrenbrink, B. (2012). Anthropogenic disturbance of element cycles at the Earth's surface. *Environmental Science & Technology*, *46*(16), 8601–8609. https://doi.org/10.1021/es301261x

Silvester, W. B. (1989). Molybdenum limitation of asymbiotic nitrogen fixation in forests of Pacific Northwest America. *Soil Biology and Biochemistry*, *21*(2), 283–289. https://doi.org/10.1016/0038-0717(89)90106-5

Smichowski, P., Gómez, D. R., Dawidowski, L. E., Giné, M. F., Bellato, A. C. S., & Reich, S. L. (2004). Monitoring trace metals in urban aerosols from Buenos Aires city. Determination by plasma-based techniques. *Journal of Environmental Monitoring*, *6*(4), 286–294. https://doi.org/10.1039/b312446k

Spiro, P. A., Jacob, D. J., & Logan, J. A. (1992). Global inventory of sulfur emissions with 1° × 1° resolution. *Journal of Geophysical Research*, *97*(D5), 6023–6036. https://doi.org/10.1029/91JD03139

Swap, R. J., Annegarn, H. J., Suttles, J. T., Haywood, J., Helmlinger, M. C., Hely, C., et al. (2002). The Southern African Regional Science Initiative (SAFARI 2000): Overview of the dry season field campaign. *South African Journal of Science*, *98*(3–4), 125–130.

Sylvestre, A., Mizzi, A., Mathiot, S., Masson, F., Jaffrezo, J. L., Dron, J., et al. (2017). Comprehensive chemical characterization of industrial PM$_{2.5}$ from steel industry activities. *Atmospheric Environment*, *152*, 180–190. https://doi.org/10.1016/j.atmosenv.2016.12.032

Taylor, S. R., & McLennan, S. M. (1995). The geochemical evolution of the continental crust. *Reviews of Geophysics*, *33*(2), 241. https://doi.org/10.1029/95RG00262

Thornton, P. E., Doney, S. C., Lindsay, K., Moore, J. K., Mahowald, N., Randerson, J. T., et al. (2009). Carbon-nitrogen interactions regulate climate-carbon cycle feedbacks: Results from an atmosphere-ocean general circulation model. *Biogeosciences*, *6*(10), 2099–2120. https://doi.org/10.5194/bg-6-2099-2009

Thorpe, A., & Harrison, R. M. (2008). Sources and properties of non-exhaust particulate matter from road traffic: A review. *Science of the Total Environment*, *400*(1–3), 270–282. https://doi.org/10.1016/j.scitotenv.2008.06.007

Van den Boogaart, K.G. and Tolosana-Delgado, R., (2008). "Compositions": a unified R package to analyze compositional data. *Computers & Geosciences*, *34*(4), pp.320–338.

Van den Boogaart, K. G., Tolosana-Delgado, R., & Bren, M. (2014). *Compositions: Compositional data analysis. R package version 1.40-1* (Vol. 34, pp. 320–338). https://CRAN.R-project.org/package=compositions

van der Werf, G. R., Randerson, J., Collatz, G. J., Giglio, L., Kasibhatla, P., Arrellano, A., et al. (2004). Continental-scale partitioning of fire emissions during the 1997 to 2001 El Nino/La Nina period. *Science*, *303*(5654), 73–76. https://doi.org/10.1126/science.1090753

Vanderzalm, J. L., Hooper, M. A., Ryan, B., Maenhaut, W., Martin, P., Rayment, P. R., & Hooper, B. M. (2003). Impact of seasonal biomass burning on air quality in the 'Top End' of regional Northern Australia. *Clean Air and Environmental Quality*, *37*(3), 28–34.

Van Dingenen, R., Raes, F., Putaud, J. P., Baltensperger, U., Charron, A., Facchini, M. C., et al. (2004). A European aerosol phenomenology—1: Physical characteristics of particulate matter at kerbside, urban, rural and background sites in Europe. *Atmospheric Environment*, *38*(16), 2561–2577. https://doi.org/10.1016/j.atmosenv.2004.01.040

Van Marle, M. J. E., Kloster, S., Magi, B. I., Marlon, J. R., Daniau, A. L., Field, R. D., et al. (2017). Historic global biomass burning emissions for CMIP6 (BB4CMIP) based on merging satellite observations with proxies and fire models (1750–2015). *Geoscientific Model Development*, *10*(9), 3329–3357. https://doi.org/10.5194/gmd-10-3329-2017

Virkkula, A., Aurela, M., Hillamo, R., Mäkelä, T., Pakkanen, T., Kerminen, V.-M., et al. (1999). Chemical composition of atmospheric aerosol in the European subarctic: Contribution of the Kola Peninsula smelter areas, central Europe, and the Arctic Ocean. *Journal of Geophysical Research*, *104*(D19), 23681–23696. https://doi.org/10.1029/1999JD900426

Vitousek, P., & Howarth, R. (1991). Nitrogen limitation on land and in the sea: How can it occur? *Biogeochemistry*, *13*(2), 87–115. https://doi.org/10.1007/BF00002772

Voutsa, D., & Samara, C. (2002). Labile and bioaccessible fractions of heavy metals in the airborne particulate matter from urban and industrial areas. *Atmospheric Environment*, *36*(22), 3583–3590. https://doi.org/10.1016/S1352-2310(02)00282-0

Wang, Y.-P., & Houlton, B. Z. (2009). Nitrogen constraints on terrestrial carbon uptake: Implications for the global carbon-climate feedback. *Geophysical Research Letters*, *36*(24), L24403. https://doi.org/10.1029/2009GL041009

Wong, M. Y., Mahowald, N. M., Marino, R., Williams, E. R., Chellam, S., & Howarth, R. W. (2020b). Natural atmospheric deposition of molybdenum: A global model and implications for tropical forests. *Biogeochemistry*, *149*(2), 159–174. https://doi.org/10.1007/s10533-020-00671-w

Wong, M. Y., Neill, C., Marino, R., Silvério, D., & Howarth, R. W. (2020a). Molybdenum, phosphorus, and pH do not constrain nitrogen fixation in a tropical forest in the southeastern Amazon. *Ecology*, *102*(1), e03211. https://doi.org/10.1002/ecy.3211

Wurzburger, N., Bellenger, J. P., Kraepiel, A. M. L., & Hedin, L. O. (2012). Molybdenum and phosphorus interact to constrain asymbiotic nitrogen fixation in tropical forests. *PloS One*, *7*(3), 1–7. https://doi.org/10.1371/journal.pone.0033710

Xiao, Y. H., Liu, S. R., Tong, F. C., Kuang, Y. W., Chen, B. F., & Guo, Y. D. (2014). Characteristics and sources of metals in TSP and PM$_{2.5}$ in an urban forest park at Guangzhou. *Atmosphere*, *5*(4), 775–787. https://doi.org/10.3390/atmos5040775

Yu, H., Chin, M., Yuan, T., Bian, H., Remer, L. A., Prospero, J. M., et al. (2015). The fertilizing role of African dust in the Amazon rainforest: A first multiyear assessment based on data from Cloud-Aerosol Lidar and Infrared Pathfinder Satellite Observations. *Geophysical Research Letters*, *42*(6), 1984–1991. https://doi.org/10.1002/2015GL063040

Zender, C., Bian, H., & Newman, D. (2003). Mineral Dust Entrainment and Deposition (DEAD) model: Description and 1990s dust climatology. *Journal of Geophysical Research*, *108*(D14), 4416. https://doi.org/10.1029/2002JD002775

Zhang, X., McRose, D. L., Darnajoux, R., Bellenger, J. P., Morel, F. M. M., & Kraepiel, A. M. L. (2016). Alternative nitrogenase activity in the environment and nitrogen cycle implications. *Biogeochemistry*, *127*(2–3), 189–198. https://doi.org/10.1007/s10533-016-0188-6

Zheng, M., Zhang, W., Luo, Y., Li, D., Wang, S., Huang, J., et al. (2018). Stoichiometry controls asymbiotic nitrogen fixation and its response to nitrogen inputs in a nitrogen-saturated forest. *Ecology*, *99*(9), 2037–2046. https://doi.org/10.1002/ecy.2416

Zheng, M., Zhou, Z., Zhao, P., Luo, Y., Ye, Q., Zhang, K., et al. (2020). Effects of human disturbance activities and environmental change factors on terrestrial nitrogen fixation. *Global Change Biology*, *26*(11), 6203–6217. https://doi.org/10.1111/gcb.15328